AD-A164 075 INVESTIGATION OF OPTICAL FIBERS FOR NONLINEAR OPTICS (U) HUGHES RESEARCH LABS MALIBU CA L DESHAZER ET AL. NOV 85 AFOSR-TR-86-0009 F49620-84-C-0043 1/1

UNCLASSIFIED F/G 20/6 NL

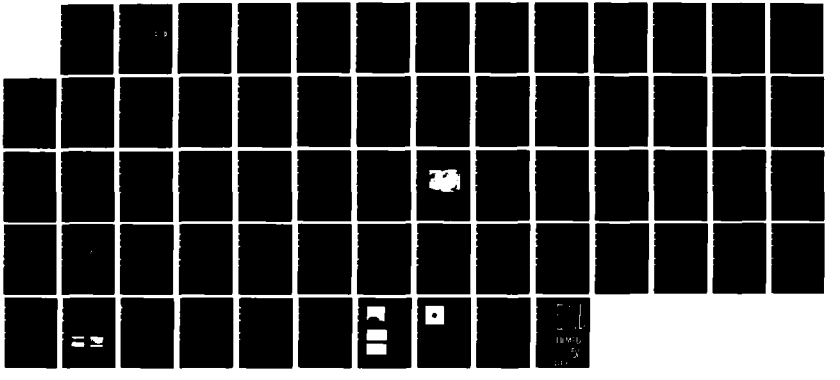

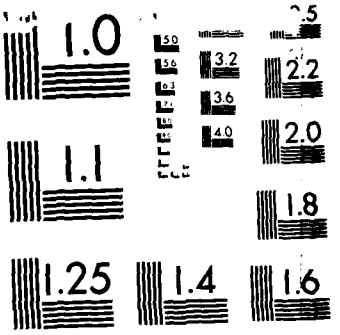

INVESTIGATION OF OPTICAL FIBERS FOR NONLINEAR OPTICS

L.G. DeShazer, A.C. Pastor, and S.C. Rand

Hughes Research Laboratories
3011 Malibu Canyon Road
Malibu, CA 90265

November 1985

F49620-84-C-0043
Annual Report
1 April 1984 through 31 March 1985

U.S. AIR FORCE OFFICE OF SCIENTIFIC RESEARCH
Bolling Air Force Base, DC 20332

UNCLRSSIFIED

SECURITY CLASSIFICATION OF THIS PAGE

AD-A164 075

REPORT DOCUMENTATION PAGE

1a. REPORT SECURITY CLASSIFICATION UNCLASSIFIED	1b. RESTRICTIVE MARKINGS
2a. SECURITY CLASSIFICATION AUTHORITY	3. DISTRIBUTION/AVAILABILITY OF REPORT Approved for public release; distribution unlimited.
2b. DECLASSIFICATION/DOWNGRADING SCHEDULE	
4. PERFORMING ORGANIZATION REPORT NUMBER(S)	5. MONITORING ORGANIZATION REPORT NUMBER(S) AFOSR-TR- 86-0009
6a. NAME OF PERFORMING ORGANIZATION Hughes Research Laboratories 6b. OFFICE SYMBOL (If applicable)	7a. NAME OF MONITORING ORGANIZATION USAF, AFSC, Bolling AFB, DC 20332
6c. ADDRESS (City, State and ZIP Code) 3011 Malibu Canyon Road Malibu, CA 90265	7b. ADDRESS (City, State and ZIP Code) Same as 6c
8a. NAME OF FUNDING/SPONSORING ORGANIZATION USAF, AFSC AFOSR 8b. OFFICE SYMBOL (If applicable) NE	9. PROCUREMENT INSTRUMENT IDENTIFICATION NUMBER F49620-84-C-0043
8c. ADDRESS (City, State and ZIP Code) Air Force Office of Scientific Research Bolling AFB, DC 20332	10. SOURCE OF FUNDING NOS. PROGRAM ELEMENT NO. 61102F; PROJECT NO. 2305; TASK NO. B2; WORK UNIT NO.
11. TITLE (Include Security Classification) Investigation of Optical Fibers for Nonlinear Optics	
12. PERSONAL AUTHOR(S) Larry DeShazer, Antonio Pastor, and Stephen Rand	
13a. TYPE OF REPORT Annual Report 13b. TIME COVERED FROM 4/1/84 TO 3/31/85	14. DATE OF REPORT (Yr., Mo., Day) November 1985 15. PAGE COUNT 67
16. SUPPLEMENTARY NOTATION —	
17 COSATI CODES FIELD / GROUP / SUB. GR	18. SUBJECT TERMS (Continue on reverse if necessary and identify by block number) Fiber optics, optical materials, single crystal fibers, evanescent wave coupling, hybrid fibers.

19. ABSTRACT (Continue on reverse if necessary and identify by block number)

The principal objective of this research program is to develop single-crystal (SC) fibers for use in nonlinear optical devices. This encompasses measurement of physical and chemical properties of several candidate materials, fabrication of SC fibers, and investigation of nonlinear optical applications. This report describes the successful fabrication of several SC fibers using new growth techniques and progress with hybrid fibers which show great promise for nonlinear optical applications.

20. DISTRIBUTION/AVAILABILITY OF ABSTRACT UNCLASSIFIED/UNLIMITED ☒ SAME AS RPT ☒ DTIC USERS ☐	21 ABSTRACT SECURITY CLASSIFICATION UNCLASSIFIED
22a. NAME OF RESPONSIBLE INDIVIDUAL ~~Stephen C. Rand~~ Dr Howard Schlossberg	22b TELEPHONE NUMBER (Include Area Code) ~~(213) 317-5171~~ 767-4908 22c OFFICE SYMBOL NE

DD FORM 1473, 83 APR EDITION OF 1 JAN 73 IS OBSOLETE.

UNCLASSIFIED

SECURITY CLASSIFICATION OF THIS PAGE

TABLE OF CONTENTS

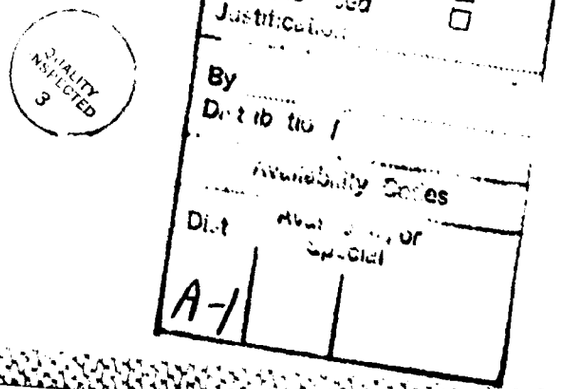

LIST OF ILLUSTRATIONS

LIST OF TABLES

SECTION 1

RESEARCH OBJECTIVES

The main objective of this contract is to find methods of fabricating optical fibers that will be useful for $\chi^{(2)}$ nonlinear devices. Successful techniques could be utilized to make nonlinear devices for frequency conversion, such as phase-matched second harmonic generation, particularly in the infrared spectrum. Device concepts and applications are to be formulated, and a theory of phase matching in fibers is also to be developed. The scope of methods investigated is intended to be broad in order to encompass at least three different candidate materials.

A variety of methods for production of single crystal (SC) fibers are to be developed, recognizing that no one method can be applied, even in principle, to SC fiber growth of all materials of interest. Efforts will be directed toward, but not limited to, the study of the following:

- Hybrid single crystal fiber method – A method of producing a glass fiber in contact with a bulk nonlinear crystal. In the presence of good optical contact between the fiber and crystal, the evanescent portion of the guided wave can interact with the nonlinear polarization of the crystal. This results in a nonlinear hybrid fiber with properties controlled by fiber diameter and orientation relative to crystal axes.

  Conditions for phase matching in hybrid fibers are to be analyzed by calculating the effective refractive indices for modes of the fundamental and second harmonic frequencies. If not available, refractive indices are to be measured in order to provide guidance for choosing fiber diameter and phase-matching geometry. New theoretical approaches are to be developed only if necessary for analysis.

- Traveling zone method – A method for converting polycrystalline (PC) fibers to SC fibers. The PC fiber is prepared by extrusion and then recrystallized into SC fiber by passing through a small melt zone. Long fiber lengths are possible for congruently melting crystals.

- Capillary-fed Czochralski method – A method for pulling SC fibers from a melt. Limitations of the conventional Czochralski process for fiber growth can be overcome by supplying the melt to the growth interface through a capillary tube. This reduces the ratio of melt surface to growth interface, minimizing the thermal problems in fiber growth, and provides the mechanical stability necessary for diameter control.

SECTION 2

STATUS OF THE RESEARCH EFFORT

A. INTRODUCTION

During the third year of the Optical Fibers for Nonlinear Optics program the technique of hybrid fibers has emerged as the most promising fiber approach to nonlinear devices. Hybrid fibers have a glass fiber core cladded with a nonlinear crystal; two methods of producing these fibers have been demonstrated. The results of the hybrid fiber approach are described in Section 2-B. In Section 2-C, our results with single crystal (SC) fiber fabrication are shown to hold promise using the capillary-fed Czochralski growth process.

B. HYBRID SINGLE CRYSTAL FIBERS

The concept of hybrid fibers was developed at HRL[1] to overcome some of the problems encountered or anticipated with early growth techniques of single crystal fibers in various optical materials. The concept of using isotropic glass fibers in conjunction with nonlinear crystals is shown in Figure 1.

12256-4R1

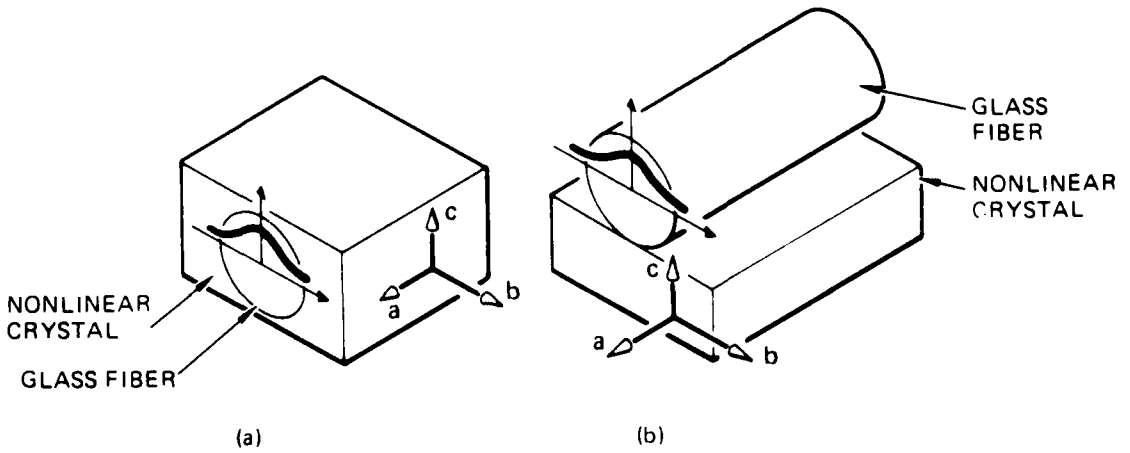

Figure 1. Two methods of utilizing evanescent waves for $\chi^{(2)}$ nonlinear processes: (a) embedded fibers; (b) proximal fibers.

Fibers in evanescent wave contact with nonlinear crystals were developed in order to combine the desirable uniformity of glass fiber waveguides with the nonlinear optical properties of bulk noncentrosymmetric crystals. The proposed operation of hybrids as nonlinear mixers and amplifiers is intended to extend the success of previous experiments[2] in planar waveguides with coupling between evanescent waves in surface guides on nonlinear crystals to the field of fiber optics. Two methods of producing hybrid fibers have been demonstrated at Hughes Research Laboratories to date.

Work in 1984 focused on the special application of hybrid fibers to noncritically phase-matched second harmonic generation (SHG). Potassium dihydrogen phosphate (KDP) isomorphs were assumed to be the nonlinear crystals to serve as cladding material and stable commercial glasses were considered for core materials. Essential properties of components such as refractive index, fiber diameter, and phase-matching geometry were identified and measured. Fibers were drawn from the most promising glass preforms. Mode propagation calculations were then performed to give the phase-matching conditions for candidate materials.

In the following two sections the measured optical properties of KDP isomorphs and commercial glasses are reported. Some of the refractive index measurements were necessary to resolve inconsistencies in reported values found in the scientific literature, while others are given here for the first time. Thermo-optic coefficients, measured with a high precision interferometric technique, were used to establish SHG wavelengths as a function of temperature. The preparation of glass waveguides is also described in Section 2-B-2. And finally, progress on the phase-matching of hybrid fibers for second harmonic generation is given in Section 2-B-3.

1. Refractive Indices and Thermo-Optic Coefficients of KDP Isomorphs

Crystals of the KDP group are widely used in nonlinear optics technology. These tetragonal isomorphs have the composition MH_2XO_4, where M may be K, Rb, Cs or NH_4; X may be P or As; and H may be fully or partially replaced by deuterium (D). They encompass 16 crystals potentially useful in state-of-the-art nonlinear optical devices. Refractive indices and their thermal variations were measured for 11 KDP isomorphs. These parameters are needed to establish the phase-matching geometry and thermal behavior of nonlinear crystals for hybrid fiber devices.

The ordinary and extraordinary indices of refraction were measured at 12 wavelengths, spanning the visible and near infrared region from 404 to 1064 nm. The measurements were obtained by the method of minimum deviation using a Gaertner spectrometer designed for this technique. The overall angular accuracy of the instrument is ±5 arc seconds, which translates to a systematic uncertainty in the refractive index of $\pm 3 \times 10^{-5}$. Crystal prisms having 1-cm faces and apex angles near 50° were furnished by Interactive Radiation, Inc. In each prism the optic axis was oriented parallel to the prism apex edge. By observing the light polarized parallel to the prism apex edge, the extraordinary index of refraction was determined. Observing the light polarized perpendicular to the edge determined the ordinary index. Tables 1 through 12 list the indices of refraction for 12 of the 16 crystals isomorphic to KDP.

The measured indices of refraction were fitted to a two-resonance Sellmeier formula,

$$n^2 = A + CB/[C\lambda^2 - 1] + D\lambda^2/[E\lambda^2 - 1] \quad , \qquad (1)$$

with deviations between measured and calculated values consistent with the estimated systematic error. The Sellmeier constants, A, B, C, D, and E are listed in Tables 1 through 12 with units appropriate for the wavelength in centimeter.

Table 1. Refractive Indices of KDP with Respect to Air at T=33.0 ± 0.4°C

(a) Measured indices and deviation of fitted indices

λ (Å)	Source	n_o	Δn_o ($\times 10^5$)	n_e	Δn_e ($\times 10^5$)
4046.56	Hg	1.52323	-1	1.47925	-8
4358.33	Hg	1.51963	1	1.47635	-2
4555.26	Cs	1.51779		1.47486	
4678.15	Cd	1.51665	3	1.47386	10
4799.91	Cd	1.51570	1	1.47314	4
5085.82	Cd	1.51365	-3	1.47150	5
5350.46	Tl	1.51195		1.47019	
5460.74	Hg	1.51137	-6	1.46983	-6
5790.66	Hg	1.50970		1.46862	
5893.00	Na	1.50897	10	1.46808	2
6438.47	Cd	1.50671	-2	1.46644	-2
7800.27	Rb	1.50201	-5	1.46358	-10
7947.60	Rb	1.50154	3	1.46328	-5
8521.13	Cs	1.49975	5	1.46230	6
8943.46	Cs	1.49854	5	1.46173	5
10640.00	Xe arc + IF	1.49383	2	1.45989	-1

(b) Sellmeier coefficients from least squares fitting

Index	Sellmeier coefficients A	B,C	D,E
Ordinary	A = 2.257574	$B = 1.0115308 \times 10^{-10}$	$D = 3.043721 \times 10^6$
		$C = 7.0637619 \times 10^9$	$E = 1.727179 \times 10^6$
Extraordinary	A = 2.129495	$B = 9.6503229 \times 10^{-11}$	$D = 5.924875 \times 10^5$
		$C = 7.2513618 \times 10^{10}$	$E = 7.870713 \times 10^5$

*Table 2. Refractive Indices of KD*P with Respect to Air at T=33.0±0.4° C*

(a) Measured indices and deviation of fitted indices

λ (Å)	Source	n_o	Δn_o ($\times 10^5$)	n_e	Δn_e ($\times 10^5$)
4046.56	Hg	1.51770	-2	1.47696	3
4358.33	Hg	1.51427	1	1.47412	-1
4678.15	Cd	1.51147	4	1.47174	3
4799.91	Cd	1.51055	4	1.47099	1
5085.82	Cd	1.50870	-1	1.46945	-5
5460.74	Hg	1.50662	-1	1.46774	-6
5893.00	Na	1.50472	-8	1.46610	-2
6438.47	Cd	1.50263	-3	1.46449	-2
7800.27	Rb	1.49882	-1	1.46162	6
7947.60	Rb	1.49840	6	1.46146	-1
8521.13	Cs	1.49721	-1	1.46057	4
8943.46	Cs	1.49629	4	1.46007	-1
10640.00	Xe arc + IF	1.49314	-3	1.45824	-2

(b) Sellmeier coefficients from least squares fitting

Index	Sellmeier coefficients A	B,C	D,E
Ordinary	A = 2.240921	$B = 9.6763930 \times 10^{-11}$	$D = 1.770363 \times 10^{6}$
		$C = 6.4019860 \times 10^{9}$	$E = 7.878938 \times 10^{5}$
Extraordinary	A = 2.126019	$B = 8.5784088 \times 10^{-11}$	$D = 6.356423 \times 10^{5}$
		$C = 8.3393628 \times 10^{9}$	$E = 8.103504 \times 10^{5}$

Table 3. Refractive Indices of ADP with Respect to Air at T=33.0 ± 0.5°C

(a) Measured indices and deviation of fitted indices

λ (Å)	Source	n_o	Δn_o ($\times 10^5$)	n_e	Δn_e ($\times 10^5$)
4046.56	Hg	1.53885	2	1.49141	-2
4358.33	Hg	1.53497	2	1.48810	2
4678.15	Cd	1.53171	0	1.48540	2
4799.91	Cd	1.53065	-2	1.48452	1
5085.82	Cd	1.52835	-2	1.48268	-1
5460.74	Hg	1.52588	-4	1.48062	2
5893.00	Na	1.52331	7	1.47875	-4
6438.47	Cd	1.52076	-2	1.47678	-4
7800.27	Rb	1.51534	3	1.47316	-5
7947.60	Rb	1.51490	-6	1.47278	1
8521.13	Cs	1.51285	1	1.47155	7
8943.46	Cs	1.51143	1	1.47078	4
10640.00	Xe arc + IF	1.50866	nf	1.46795	-2

nf = measurement not used in Sellmeier fit

(b) Sellmeier coefficients from least squares fitting

Index	Sellmeier coefficients A	B,C	D,E
Ordinary	A = 2.301929	$B = 1.0569191 \times 10^{-10}$ $C = 5.6024115 \times 10^{9}$	$D = 3.810084 \times 10^{6}$ $E = 2.137123 \times 10^{6}$
Extraordinary	A = 2.162273	$B = 9.8656652 \times 10^{-11}$ $C = 9.6615997 \times 10^{9}$	$D = 1.423869 \times 10^{6}$ $E = 7.807344 \times 10^{5}$

*Table 4. Refractive Indices of AD*P with Respect to Air at T=33.0 ± 0.5°C*

(a) Measured indices and deviation of fitted indices

λ (Å)	Source	n_o	Δn_o ($\times 10^5$)	n_e	Δn_e ($\times 10^5$)
4046.56	Hg	1.53207	-3	1.50519	-6
4358.33	Hg	1.52830	7	1.50185	1
4678.15	Cd	1.52535	-1	1.49911	3
4799.91	Cd	1.52433	0	1.49819	4
5085.82	Cd	1.52226	-2	1.49631	2
5460.74	Hg	1.51995	-1	1.49424	0
5893.00	Na	1.51775	0	1.49225	1
6438.47	Cd	1.51554	-7	1.49025	-2
7800.27	Rb	1.51119	-1	1.48653	-1
7947.67	Rb	1.51065	14	1.48614	6
8521.13	Cs	1.50938	-4	1.48513	-10
8943.46	Cs	1.50837	-3	1.48427	-3
10640.00	Xe arc + IF	1.50461	0	1.48139	5

(b) Sellmeier coefficients from least squares fitting

Index	Sellmeier coefficients A	B,C	D,E
Ordinary	A = 2.278200	$B = 1.0956056\times10^{-10}$	$D = 2.114247\times10^{6}$
		$C = 8.0185605\times10^{9}$	$E = 7.811149\times10^{5}$
Extraordinary	A = 2.199071	$B = 1.1105910\times10^{-10}$	$D = 1.244920\times10^{6}$
		$C = 7.2515101\times10^{10}$	$E = 7.865980\times10^{5}$

Table 5. Refractive Indices of CDA with Respect to Air at T=33.0 ± 0.5°C

(a) Measured indices and deviation of fitted indices

λ (Å)	Source	n_o	Δn_o ($\times 10^5$)	n_e	Δn_e ($\times 10^5$)
4046.56	Hg	1.59003	-4	1.56669	-3
4358.33	Hg	1.58440	-3	1.56159	0
4678.15	Cd	1.57987	3	1.55744	5
4799.91	Cd	1.57837	5	1.55612	3
5085.82	Cd	1.57535	0	1.55338	1
5460.74	Hg	1.57206	-5	1.55052	-8
5893.00	Na	1.56894	-7	1.54776	-4
6438.47	Cd	1.56568	-1	1.54502	2
7800.27	Rb	1.55981	1	1.54060	-4
7947.67	Rb	1.55931	-1	1.54016	4
8521.13	Cs	1.55735	6	1.53892	2
8943.46	Cs	1.55610	3	1.53810	3
10640.00	Xe arc + IF	1.55148	-3	1.53564	-2

(b) Sellmeier coefficients from least squares fitting

Index	Sellmeier coefficients A	B.C	D,E
Ordinary	A = 2.420405	$B = 1.6272261 \times 10^{-10}$ $C = 5.5538145 \times 10^{9}$	$D = 2.426902 \times 10^{6}$ $E = 1.729381 \times 10^{6}$
Extraordinary	A = 2.350262	$B = 1.5645403 \times 10^{-10}$ $C = 6.7472517 \times 10^{9}$	$D = 5.384884 \times 10^{5}$ $E = 7.857386 \times 10^{5}$

*Table 6. Refractive Indices of CD*A with Respect to Air at T=33.0±0.4° C*

(a) Measured indices and deviation of fitted indices

λ (Å)	Source	n_o	Δn_o ($\times 10^5$)	n_e	Δn_e ($\times 10^5$)
4046.56	Hg	1.58529	0	1.56464	-2
4358.33	Hg	1.57990	2	1.55954	4
4678.15	Cd	1.57562	-5	1.55553	-1
4799.91	Cd	1.57419	-3	1.55421	-1
5085.82	Cd	1.57122	1	1.55148	0
5460.74	Hg	1.56801	6	1.54856	2
5893.00	Na	1.56512	1	1.54593	-2
6438.47	Cd	1.56218	-1	1.54330	-1
7800.27	Rb	1.55701	-10	1.53896	-4
7947.60	Rb	1.55646	0	1.53854	3
8521.13	Cs	1.55476	7	1.53735	-1
8943.46	Cs	1.55371	3	1.53652	4
10640.00	Xe arc + IF	1.54995	-3	1.53413	-1

(b) Sellmeier coefficients from least squares fitting

Index	Sellmeier coefficients A	B,C	D,E
Ordinary	A = 2.408170	$B = 1.5597934 \times 10^{-10}$	$D = 1.743638 \times 10^6$
		$C = 5.2351416 \times 10^9$	$E = 7.882014 \times 10^5$
Extraordinary	A = 2.345809	$B = 1.5141459 \times 10^{-10}$	$D = 5.119295 \times 10^5$
		$C = 5.9396419 \times 10^9$	$E = 7.853574 \times 10^5$

Table 7. Refractive Indices of ADA with Respect to Air at 33.0 ± 0.5°C

(a) Measured indices and deviation of fitted indices

λ (Å)	Source	n_o	Δn_o ($\times 10^5$)	n_e	Δn_e ($\times 10^5$)
4046.56	Hg	1.59779	-1	1.53984	-3
4358.33	Hg	1.59199	-1	1.53489	4
4678.15	Cd	1.58722	2	1.53098	-1
4799.91	Cd	1.58567	1	1.52968	0
5085.82	Cd	1.58243	0	1.52700	1
5460.74	Hg	1.57885	3	1.52413	0
5893.00	Na	1.57553	-3	1.52147	-2
6438.47	Cd	1.57204	-5	1.51879	-3
7800.27	Rb	1.56537	0	1.51406	1
7947.60	Rb	1.56472	4	1.51366	1
8521.13	Cs	1.56250	2	1.51225	0
8943.46	Cs	1.56097	-1	1.51131	1
10640.00	Xe arc + IF	1.55507	-1	1.50812	-1

(b) Sellmeier coefficients from least squares fitting

Index	Sellmeier coefficients A	B,C	D,E
Ordinary	A = 2.443449	$B = 1.6756541 \times 10^{-10}$	$D = 3.488801 \times 10^6$
		$C = 5.4726728 \times 10^9$	$E = 1.729053 \times 10^6$
Extraordinary	A = 2.275962	$B = 1.4296386 \times 10^{-10}$	$D = 1.259613 \times 10^6$
		$C = 6.0383457 \times 10^9$	$E = 7.881151 \times 10^5$

*Table 8. Refractive Indices of AD*A with Respect to Air at T=33.0 ± 0.5°C*

(a) Measured indices and deviation of fitted indices

λ (Å)	Source	n_o	Δn_o (x10^5)	n_e	Δn_e (x10^5)
4046.56	Hg	1.59056	nf	1.53586	nf
4358.33	Hg	1.58487	1	1.53102	5
4678.15	Cd	1.58036	-2	1.52722	-5
4799.91	Cd	1.57889	-4	1.52593	-3
5085.82	Cd	1.57580	-1	1.52331	-1
5460.74	Hg	1.57242	3	1.52050	0
5893.00	Na	1.56921	11	1.51785	7
6438.47	Cd	1.56619	-4	1.51538	-1
7800.27	Rb	1.56045	-4	1.51103	-1
7947.67	Rb	1.55991	-1	1.51063	3
8521.13	Cs	1.55808	-1	1.50944	-5
8943.46	Cs	1.55683	1	1.50856	1
10640.00	Xe arc + IF	1.55237	2	1.50587	1

nf = measurement not used in Sellmeier fit

(b) Sellmeier coefficients from least squares fitting

Index	Sellmeier coefficients A	B,C	D,E
Ordinary	A = 2.413739	$B = 1.9040362 \times 10^{-10}$	$D = 1.741336 \times 10^{6}$
		$C = 4.1206727 \times 10^{10}$	$E = 1.679311 \times 10^{6}$
Extraordinary	A = 2.259082	$B = 1.6092255 \times 10^{-10}$	$D = 4.502676 \times 10^{5}$
		$C = 3.800927 \times 10^{10}$	$E = 2.405449 \times 10^{6}$

Table 9. Refractive Index of RDP with Respect to Air at T=32.9 ± 0.4°C

(a) Measured indices and deviation of fitted indices

λ (Å)	Source	n_o	Δn_o ($\times 10^5$)	n_e	Δn_e ($\times 10^5$)
4046.56	Hg	1.52078	2	1.48995	-1
4358.33	Hg	1.51741	-7	1.48689	1
4678.15	Cd	1.51447	-2	1.48439	1
4799.91	Cd	1.51343	5	1.48356	2
5085.82	Cd	1.51138	6	1.48187	0
5460.74	Hg	1.50915	2	1.48002	-1
5893.00	Na	1.50697	-2	1.47830	-2
6438.47	Cd	1.50469	-10	1.47658	-6
7800.27	Rb	1.49995	-4	1.47339	5
7947.60	Rb	1.49946	1	1.47321	-3
8521.13	Cs	1.49774	6	1.47222	3
8943.46	Cs	1.49655	7	1.47160	3
10640.0	Xe arc + IF	1.49208	-5	1.46957	-3

(b) Sellmeier coefficients from least squares fitting

Index	Sellmeier coefficients A	B,C	D,E
Ordinary	A = 2.249885	$B = 1.0559738 \times 10^{-10}$	$D = 2.899380 \times 10^6$
		$C = 1.2852642 \times 10^{10}$	$E = 7.861649 \times 10^5$
Extraordinary	A = 2.159913	$B = 9.5146863 \times 10^{-11}$	$D = 7.740684 \times 10^5$
		$C = 1.1795379 \times 10^{10}$	$E = 7.831282 \times 10^5$

*Table 10. Refractive Indices of RD*P with Respect to Air at T = 33.0 ± 0.5°C*

(a) Measured indices and deviation of fitted indices

λ (Å)	Source	n_o	Δn_o ($\times 10^5$)	n_e	Δn_e ($\times 10^5$)
4046.56	Hg	1.51655	2	1.48780	
4358.33	Hg	1.51325	-3	1.48486	0
4678.15	Cd	1.51058	2	1.48240	-1
4799.91	Cd	1.50963	-2	1.48162	-4
5085.82	Cd	1.50772	-1	1.48001	-1
5085.82	Cd	1.50772	-1	1.48001	5
5460.74	Hg	1.50555	-6	1.47814	1
5790.66	Hg	1.50410	8	1.47683	4
6438.47	Cd	1.50150	6	1.47474	5
7800.27	Rb	1.49742	1	1.47166	-4
7947.60	Rb	1.49705	0	1.47146	1
8521.13	Cs	1.49565	-5	1.47050	-7
8943.46	Cs	1.49472	-5	1.46997	-3
10640.00	Xe arc + IF	1.49136	3	1.46818	6

(b) Sellmeier coefficients from least squares fitting

Index	Sellmeier coefficients A	B,C	D,E
Ordinary	A = 2.235596	$B = 1.092894 \times 10^{-10}$ $C = 7.2513815 \times 10^{10}$	$D = 1.856709 \times 10^6$ $E = 7.883038 \times 10^5$
Extraordinary	A = 2.152727	$B = 1.0022483 \times 10^{-10}$ $C = 7.2509186 \times 10^{-10}$	$D = 5.442314 \times 10^5$ $E = 7.873119 \times 10^5$

Table 11. Refractive Index of RDA with Respect to Air at T=33.0 ± 0.5°C

(a) Measured indices and deviation of fitted indices

λ (A)	Source	n_o	Δn_o ($\times 10^5$)	n_e	Δn_e ($\times 10^5$)
4046.56	Hg	1.57882	0	1.53880	1
4358.33	Hg	1.57344	0	1.53421	1
4678.15	Cd	1.56906	-1	1.53052	-1
4799.91	Cd	1.56761	0	1.52932	-3
5085.82	Cd	1.56460	2	1.52678	2
5460.74	Hg	1.56134	1	1.52410	2
5893.00	Na	1.55827	0	1.52162	3
6438.47	Cd	1.55512	-1	1.51923	-2
7800.27	Rb	1.54926	-3	1.51511	-1
7947.60	Rb	1.54872	-2	1.51476	0
8521.13	Cs	1.54674	3	1.51360	0
8943.46	Cs	1.54541	2	1.51285	0
10640.00	Xe arc + IF	1.54052	-1	1.51047	0

(b) Sellmeier coefficients from least squares fitting

Index	Sellmeier coefficients A	B,C	D,E
Ordinary	A = 2.390661	$B = 1.5512827 \times 10^{-10}$ $C = 5.5211018 \times 10^{9}$	$D = 2.750904 \times 10^{6}$ $E = 7.888619 \times 10^{5}$
Extraordinary	A = 2.275570	$B = 1.3914908 \times 10^{-10}$ $C = 6.8528051 \times 10^{9}$	$D = 5.686596 \times 10^{5}$ $E = 7.896963 \times 10^{5}$

Table 12. Refractive Index of KDA with Respect to Air at T=33.0 ± 0.5°C

(a) Measured indices and deviation of fitted indices

λ (Å)	Source	n_o	Δn_o ($\times 10^5$)	n_e	Δn_e ($\times 10^5$)
4046.56	Hg	1.58714	1	1.53391	3
4358.33	Hg	1.58163	2	1.52931	-3
4678.15	Cd	1.57708	-4	1.52561	-6
4799.91	Cd	1.57559	-5	1.52448	1
5085.82	Cd	1.57257	1	1.52204	3
5460.74	Hg	1.56923	0	1.51935	-2
5790.66	Hg	1.56685	9	1.51756	9
6438.47	Cd	1.56284	2	1.51454	-1
7800.27	Rb	1.55677	2	1.51053	3
7947.60	Rb	1.55619	-1	1.51016	-1
8521.13	Cs	1.55416	-3	1.50895	-6
8943.46	Cs	1.55274	-6	1.50827	0
10640.00	Xe arc	1.54767	3	1.50591	1

(b) Sellmeier coefficients from least squares fitting

Index	Sellmeier coefficients A	B,C	D,E
Ordinary	A = 2.414647	$B = 1.5841464 \times 10^{-10}$	$D = 2.949448 \times 10^6$
		$C = 5.3694136 \times 10^9$	$E = 7.880000 \times 10^5$
Extraordinary	A = 2.262579	$B = 1.3461143 \times 10^{-10}$	$D = 6.054821 \times 10^5$
		$C = 6.1858412 \times 10^9$	$E = 7.870687 \times 10^5$

The thermo-optic coefficients, $\alpha_n = n^{-1}\, dn/dT$, of the KDP isomorphs were measured using a double interferometric technique involving the simultaneous use of the Twyman-Green and Fizeau configurations. This technique is basically the method devised by Fizeau for determining the coefficient of thermal expansion, except a Twyman-Green interferometer has been added to determine simultaneously the thermo-optic coefficient. Cabezas et al.[3] first used this double interferometric approach to measure temperatures of materials during pumping in a laser amplifier. Wilson[4] refined the method to provide accurate thermo-optic measurements for optical materials, including CD*A.[5]

The double interferometric arrangement is shown in Figure 2. Fizeau fringes are produced by interference of the two beams reflected from the almost parallel sample faces, and the Twyman-Green fringes are found by the interference of the two beams reflected from the fixed mirrors. As the sample is heated, both the Twyman-Green and Fizeau fringes move across the aperture as a result of the changing optical path length in the sample. Even though both fringe patterns are functions of α_L and α_n, the Fizeau and Twyman-Green fringe patterns change with temperature at different rates. Then α_L and α_n can be determined from measurement of these two fringe rates by the simultaneous solution of the two equations that describe the phase shifts for the two interferometers.

Crystal plates 8 x 11 x 12 mm were held in a gimbal mount in a vacuum oven which provided a linear heat ramp to the crystal from 25 to 40°C. The chamber was evacuated to 10^{-6} Torr to eliminate thermal change of the refractive index of air and heating of the oven windows by air convention. The front and rear faces of the sample were polished with 2 or 3 fringes (at 632.8 nm) of wedge between the two surfaces in order to provide a definable Fizeau fringe pattern. The lasers used for the interferometric measurements were two He-Ne lasers (Spectra-Physics) at 632.8 and 1150 nm and a He-Cd laser (Liconix) at 441.6 nm.

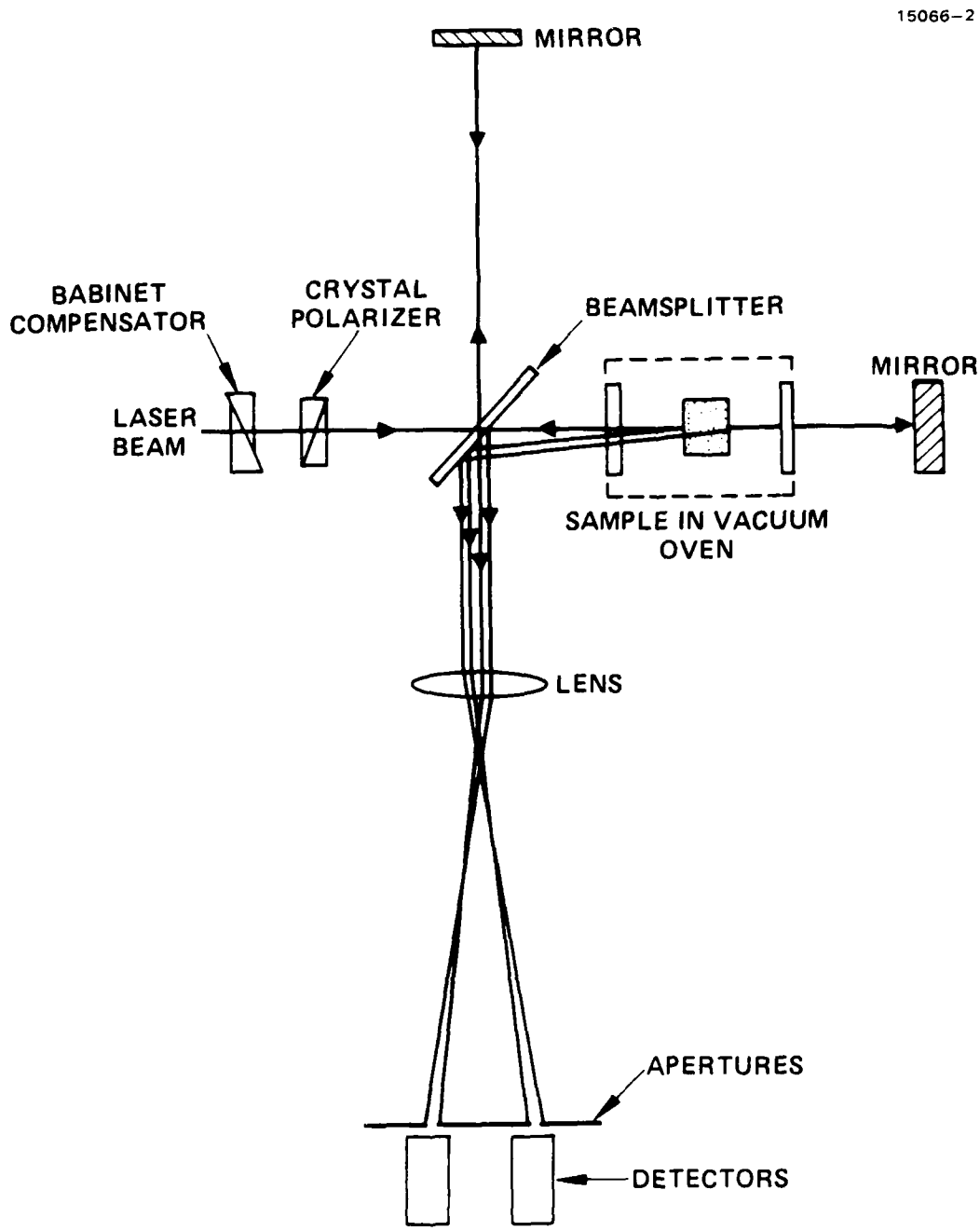

Figure 2. Double interferometry arrangement to measure thermal variation of refractive indices.

The quantities actually determined by the experiment are ΔT_T and ΔT_F, the temperature changes needed to move one fringe in the Twyman-Green and Fizeau interferograms. Each fringe pattern is magnified and sampled by a pinhole placed in front of photomultiplier detectors. As the sample is heated, the motion of each pattern across its pinhole is recorded on a dual-pen chart recorder. Then ΔT_T and ΔT_F are determined from the recording and used to calculate α_n and α_L using the relations,

$$\alpha_L = (\lambda/2L)(\Delta T_T^{-1} - \Delta T_F^{-1}) \quad (2)$$

and

$$\alpha_n = (\lambda/2L)\{\Delta T_T^{-1} - [(n-1)/n]\Delta T_F^{-1}\} \quad (3)$$

where λ is the wavelength of light and L is the length of the sample. This measurement was made for light polarized parallel (extraordinary) and perpendicular (ordinary) to the optic axis for three wavelengths (441.6, 632.8, and 1152 nm). Note that the determination of the expansion coefficient, α_L, does not depend on the refractive index, as expected, while the determination of α_n does require index values.

Table 13 lists the thermo-optic coefficients α_n for 12 KDP isomorphs. The mean deviation of the measurements was 6% for all 12 crystals.

2. Refractive Indices and Transmission Spectra of Commercial Glasses

The three glasses that have been studied as potential hybrid components are Corning 7052, Schott BK1, and Schott PK3. All are highly transmissive throughout the visible and near infrared spectral regions important to hybrid fiber operation (Figure 3), and have refractive indices higher than that of silica, as required to achieve guiding in fibers with KDP isomorph cladding. Their softening temperatures given in Table 14 are lower than that of silica glass, rendering fiber preparation much easier.

Table 13. Thermo-optic Coefficients of KDP Isomorph Crystals

Crystal	Pol	α_n (x10^{-6}/°C)		
		441.6 nm	632.8 nm	1152 nm
KDP	Ord	-26.2*	-27.9	-24.3
	Ext	-19.3*	-21.8	-20.5
KD*P	Ord	-18.5	-20.9	-19.0
	Ext	-14.8	-15.7	-15.9
ADP	Ord	-34.6*	-30.5	-30.2
	Ext	-7.5*	2.0	-2.3
AD*P	Ord	-25.5	-24.5	-26.8
	Ext	-12.9	-12.1	-13.0
CDA	Ord	-21.0	-21.1	-17.8
	Ext	-12.6	-14.7	-15.7
CD*A	Ord	-16.0	-16.7	-16.4
	Ext	-11.5	-12.3	-14.8
ADA	Ord	-29.5	-30.6	-27.4
	Ext	6.7	6.4	3.4
AD*A	Ord	-16.8	-17.0	-19.0
	Ext	-11.6	-15.2	-14.1
RDP	Ord	-24.2	-28.4	-27.6
	Ext	-18.3	-19.9	-19.9
RD*P	Ord	-2.4	-2.0	-3.7
	Ext	-3.3	-1.6	-3.5
RDA	Ord	-23.1	-19.8	-21.0
	Ext	-12.8	-15.3	-16.0
KDA	Ord	-24.4	-24.9	-23.7
	Ext	-16.2	-14.6	-15.9

*Values for 457.9 nm instead of 441.6 nm

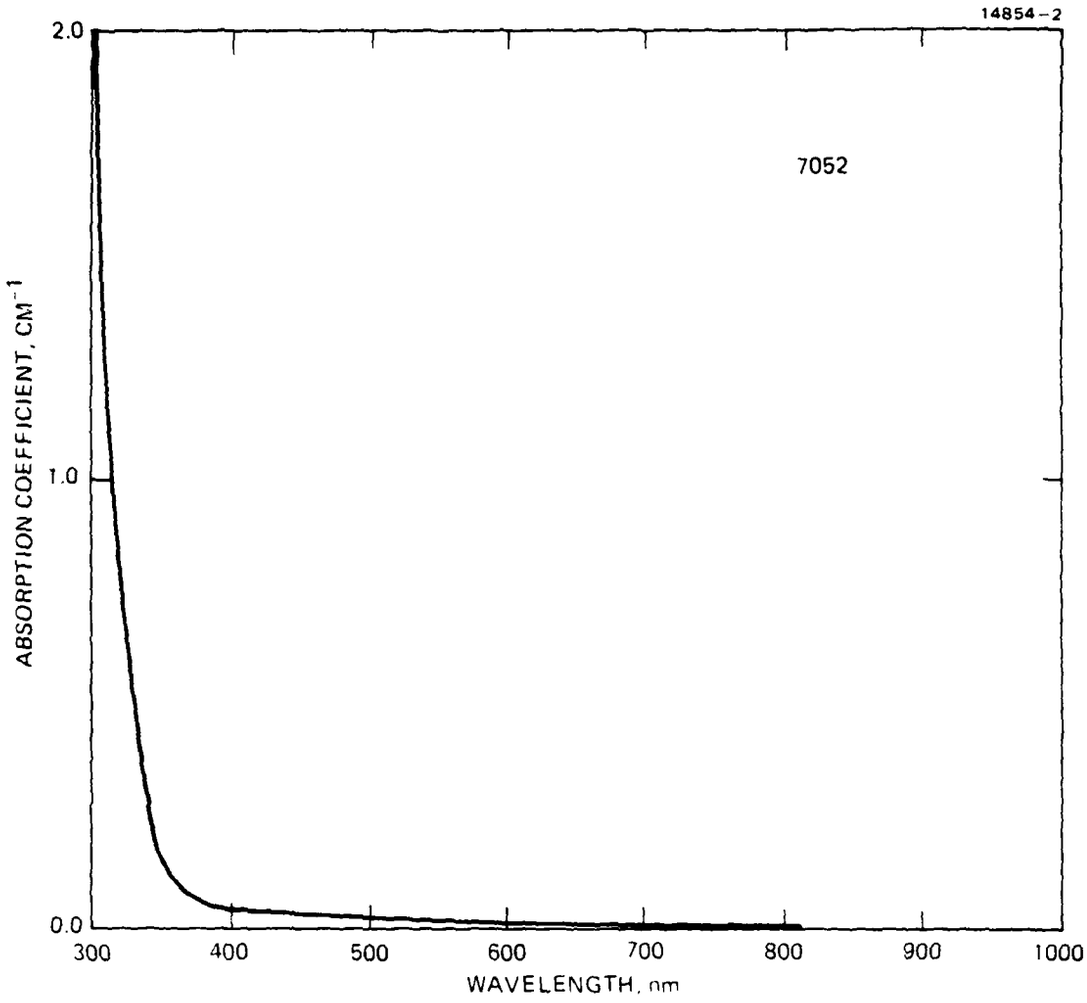

Figure 3(a). Absorption spectrum of Corning glass type 7052.

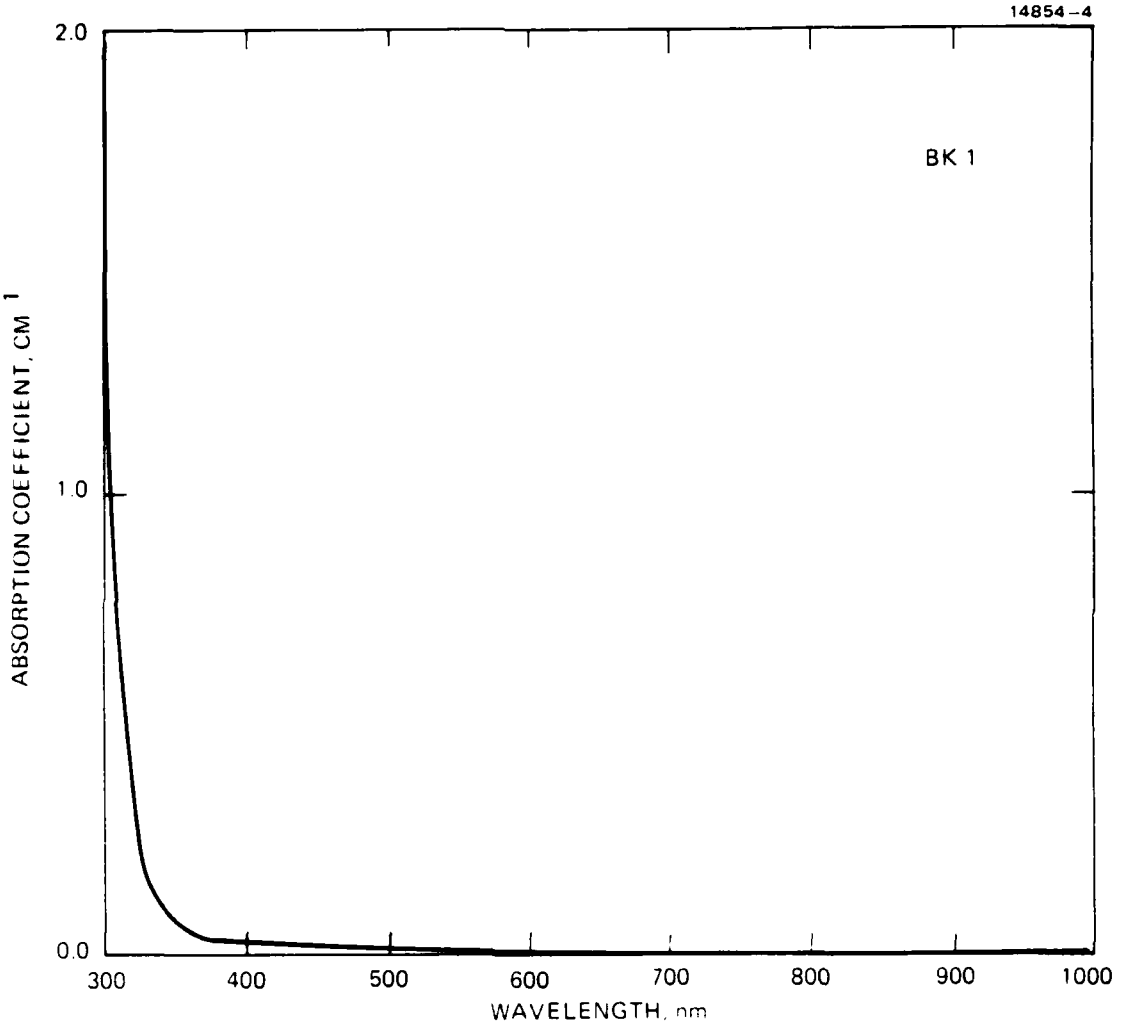

Figure 3(b). Absorption spectrum of Schott glass type BK1.

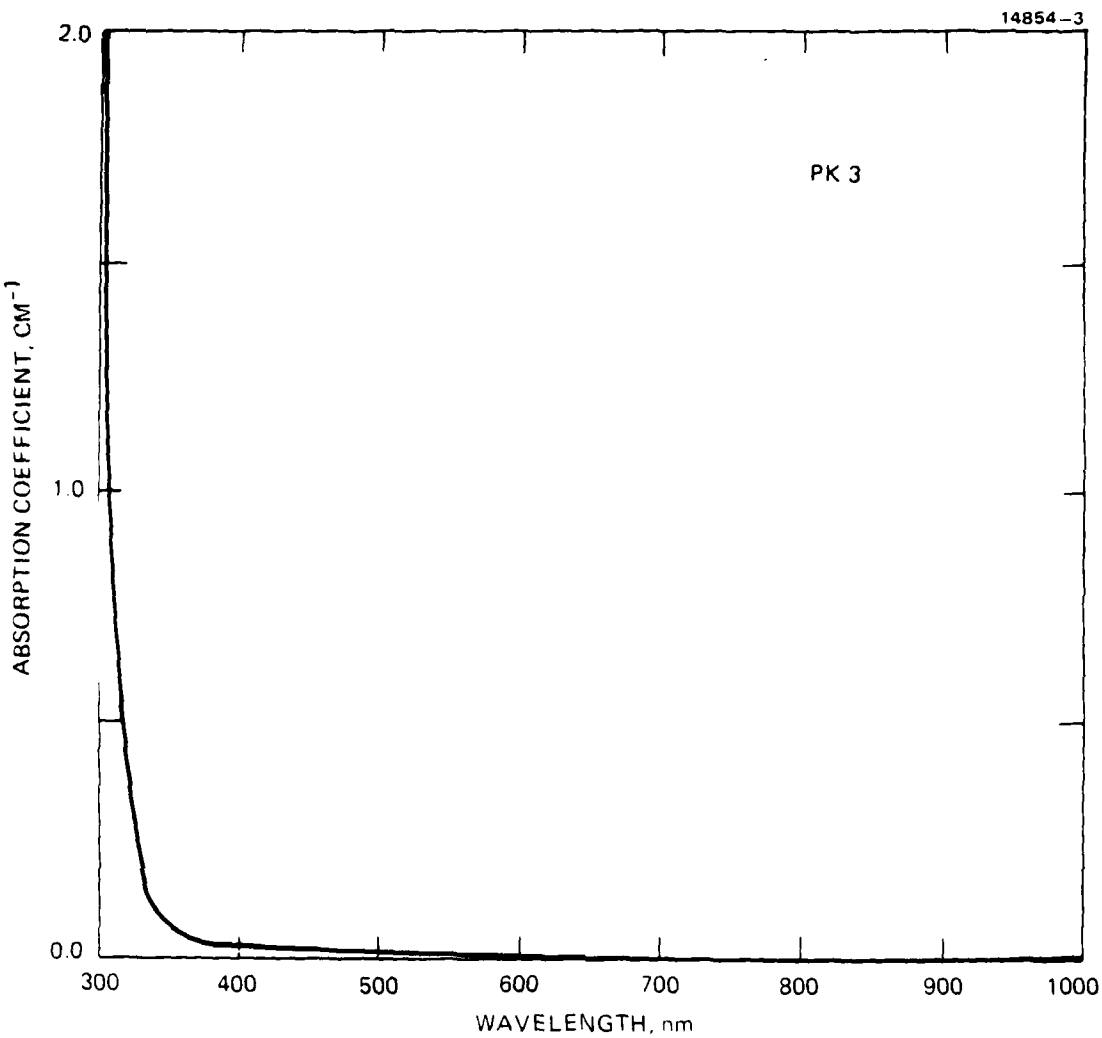

Figure 3(c). Absorption spectrum of Schott glass type PK3.

Table 14. Softening and annealing temperatures of commercial glasses

Glass	Annealing (°C)	Softening (°C)
Schott BK1	547	730
Schott PK3	567	710
Corning 7052	480	708
Corning 7911	910	1500

Measurements of refractive indices were made for these glasses using the same procedure outlined for the KDP isomorphs in the previous subsection. The results are listed in Tables 15 through 17. By comparing the index values of these tables with those for KDP and ADP (Tables 1 and 3, respectively), it is evident that

$$n(\text{BK1}) \sim n_{\emptyset}(\text{KDP}) > n_{\bullet}(\text{KDP})$$

and

$$n(\text{PK3}) \sim n_{\emptyset}(\text{ADP}) > n_{\bullet}(\text{ADP}).$$

As explained in the next section, this means that BK1/KDP and PK3/ADP combinations are attractive hybrid fiber combinations.

Optical fibers of these glasses were prepared in a standard fiber drawing tower at Hughes Research Laboratories in Malibu (Figure 4). Meter-length preforms were mounted vertically in the oven section at the top and fibers of controlled diameters from 25 to 100 μm were taken up on a large spool at floor level. Diameter measurement and active control were provided by a servo mechanism employing He-Ne diffraction patterns to monitor the drawing process. Even the smallest fibers (25 to 50 μm in diameter) could be controlled to within a 5-μm tolerance in this manner.

Table 15. 7052 Corning Glass Refractive Index

Wavelength (A)	n
4046.560	1.49425
4358.330	1.49081
4678.150	1.48824
4799.910	1.48728
5085.820	1.48553
5460.740	1.48351
7800.270	1.47640
7947.600	1.47613
8521.120	1.47505
8943.460	1.47439
10640.000	1.47201

Sellmeier Constants

A = 2.169569
B = $9.7431514 \times 10^{-11}$
C = 7.5647555×10^{9}
D = 1.008468×10^{6}
E = 7.843609×10^{5}

Table 16. PK3 Schott Glass Refractive Index

Wavelength (A)	n
4046.560	1.53473
4358.330	1.53122
4678.150	1.52829
4799.910	1.52735
5085.820	1.52539
5893.000	1.52132
6438.470	1.51941
7800.270	1.51549
7947.600	1.51512
8521.130	1.51413
8943.460	1.51327
10640.000	1.51085

Sellmeier Constants

A = 2.283683
B = $1.1675001E-10 \times 10^{-10}$
C = $2.3691721E+10 \times 10^{10}$
D = 9.993731×10^{5}
E = 1.725908×10^{6}

Table 17. BK1 Schott Glass Refractive Index

Wavelength (Å)	n
4046.560	1.52092
4358.330	1.51742
4678.150	1.51452
4799.910	1.51363
5085.820	1.51164
5460.740	1.50947
5893.000	1.50750
6438.470	1.50555
7800.270	1.50185
7947.600	1.50158
8521.130	1.50052
8943.460	1.49976
10640.000	1.49746

Sellmeier Constants

A = 2.241714
B = $1.1515248 \times 10^{-10}$
C = 1.7639387×10^{10}
D = 8.425489×10^{5}
E = 7.880428×10^{5}

Figure 4. Glass fiber drawing towers at HRL.

3. Phase-Matching Conditions

Phase-matched SHG in waveguides with active cladding can be achieved when a low order mode of the fundamental has the same propagation constant ("effective" refractive index in the guide) as a low order mode at the second harmonic frequency. This permits the exchange of energy through the cladding $\chi^{(2)}$ nonlinearity. Hence, one needs to calculate the effective refractive indices for modes of the fundamental and second harmonic frequencies and to determine their intersection points. This must be done for a cladding which furnishes "weak" guiding as well as the requisite nonlinear response. In addition, to achieve long interaction lengths for SHG, non-critical phase-matching is desirable. Only geometries in which ordinary and extraordinary polarizations have parallel Poynting vectors should be considered.

We have prepared extensive computer codes to solve the complex eigenvalue problem determining the mode structure in hybrid optical fibers. It should be emphasized that this mode propagation problem for the case in which the cladding exhibits birefringence has not been solved or modelled previously. The equation from which mode dispersion may be calculated is[6]

$$u[J_{-1}(u)/J_{}(u)] = -w[K_{-1}(w)/K_{}(w)] \qquad (4)$$

where

$$u = a(\kappa^2 n_c^2 - \beta^2)^{1/2},$$

$$w = a(\beta^2 - \kappa^2 n^2)^{1/2},$$

β = propagation constant, a = core radius, and n and n_c are the refractive indices of the cladding and core respectively.

Solutions of this equation are illustrated in Figure 5 for a fiber core made of 7052 glass in a hypothetical nonlinear medium set to have an index smaller by $\Delta n = 10^{-4}$. Only the lowest order modes are labeled. Three intersections of the solid and dashed curves may be noted, yielding three values of a/λ for which SHG can occur. These values are roughly 15.5, 25.7, and 47.0, and were calculated for a fixed fiber diameter of 50 μm. In this hybrid fiber the low order intersection points useful for SHG occur at the three wavelengths:

$$\lambda_1 = 1.610\ \mu m,$$

$$\lambda_2 = 0.973\ \mu m,$$

and

$$\lambda_3 = 0.532\ \mu m.$$

An important feature of the solutions may be noted from Figure 5. Because the refractive index of materials transparent at visible and near infrared wavelengths invariably increases for decreasing wavelength, the $(01)_{2\omega}$ mode never intersects the $(01)_{\omega}$ mode. Hence, SHG will always occur with propagation in higher order modes. Moreover, although a fiber might be designed to be single mode at frequency ω, it would generally be multimode at frequency 2ω. Second harmonic generation is therefore inherently a multimode fiber problem with multimode fiber applications. This is not true, however, of three-wave mixing in general in these fibers.

In Figures 6 and 7 we present calculated dispersion curves similar to Figure 5 for PK3/ADP and BK1/KDP hybrid fibers, based on the measured properties of component materials. Again, intersection points are clearly seen among the low order modes of fundamental and second harmonic modes. However, in this case the curves were calculated for fixed wavelength $\lambda = 1.06\ \mu m$ of the fundamental wave; intersections give the fiber radius necessary to phase-match second harmonic generation of 1.06-μm light. The

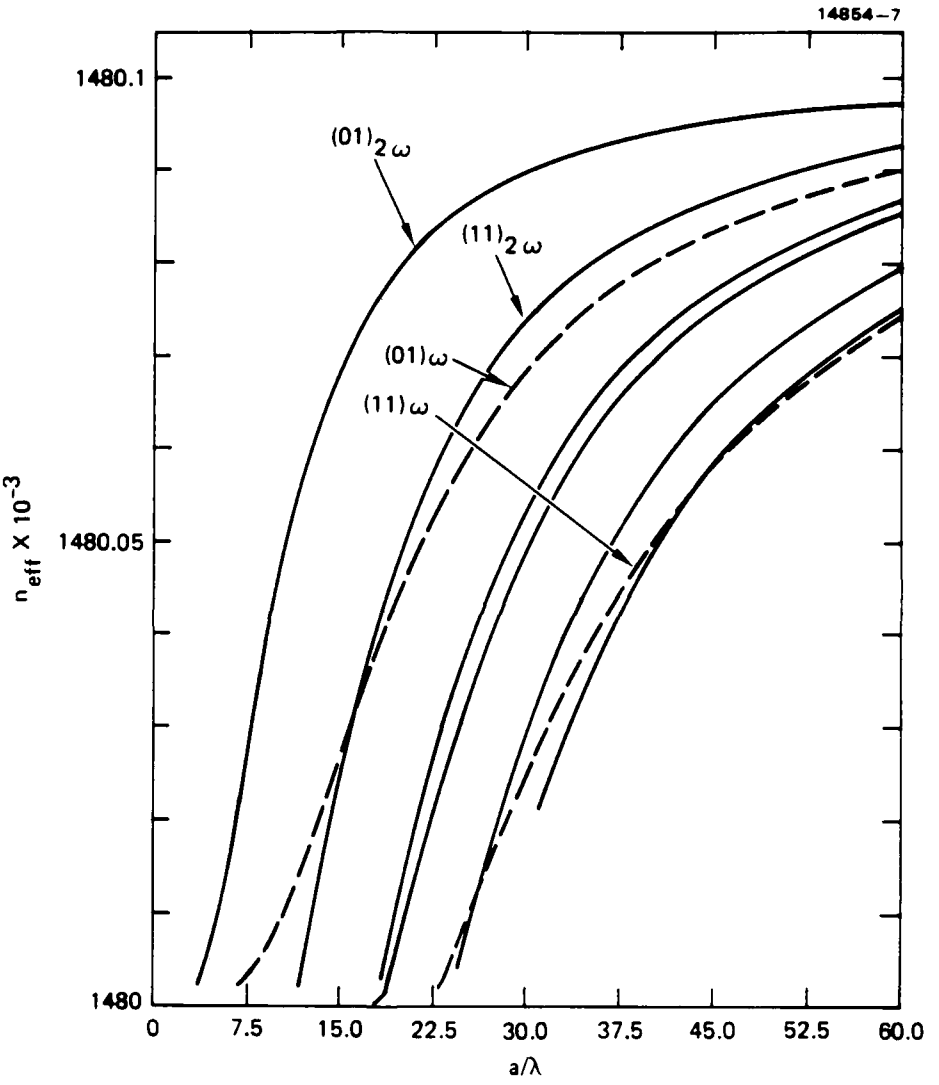

Figure 5. Dispersion curves for hybrid fiber with 7052 glass core: a=25μm, $\Delta n=10^{-4}$.

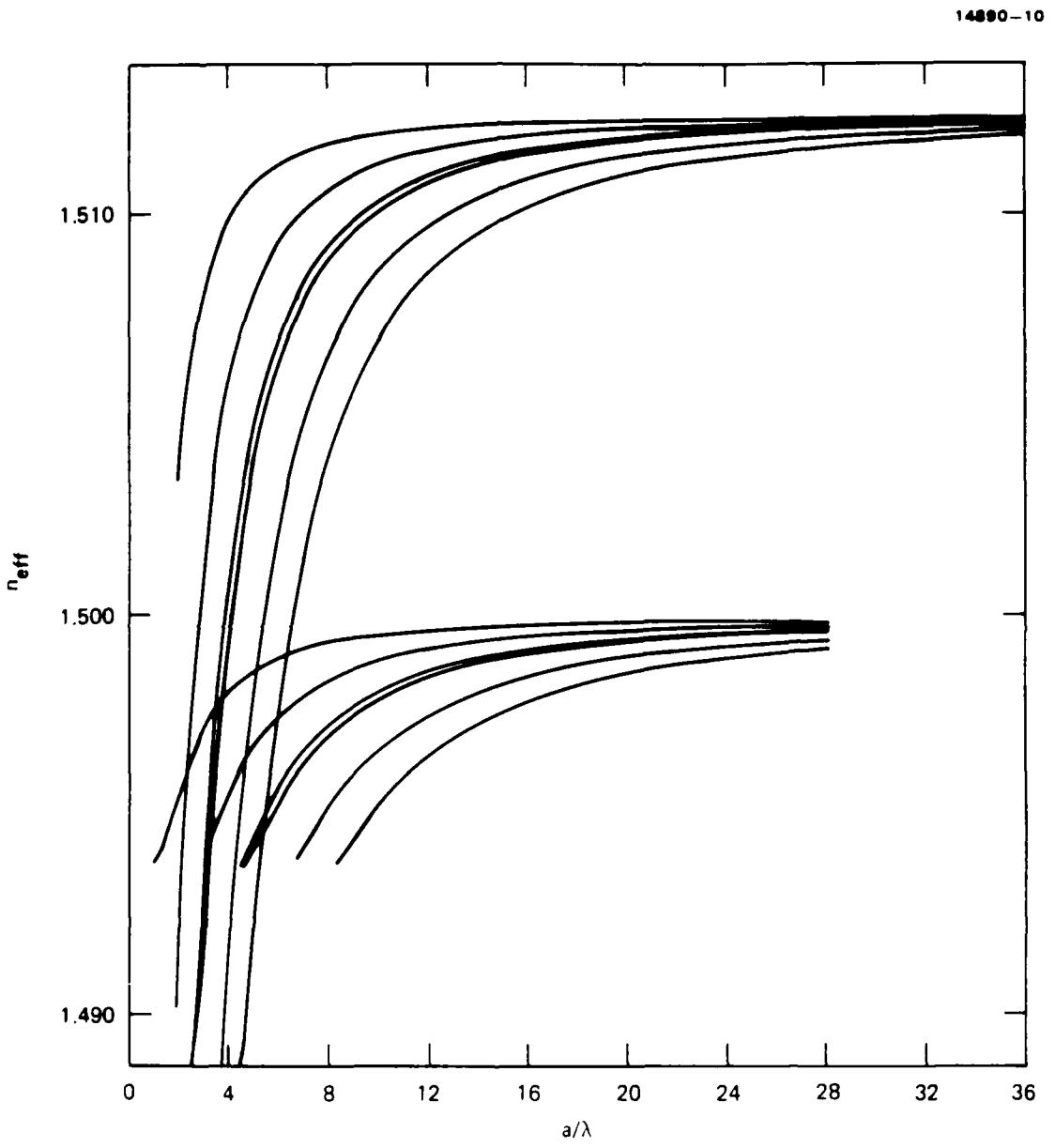

Figure 6. Dispersion curves for hybrid fiber with BK1 glass fiber embedded in a KDP crystal.

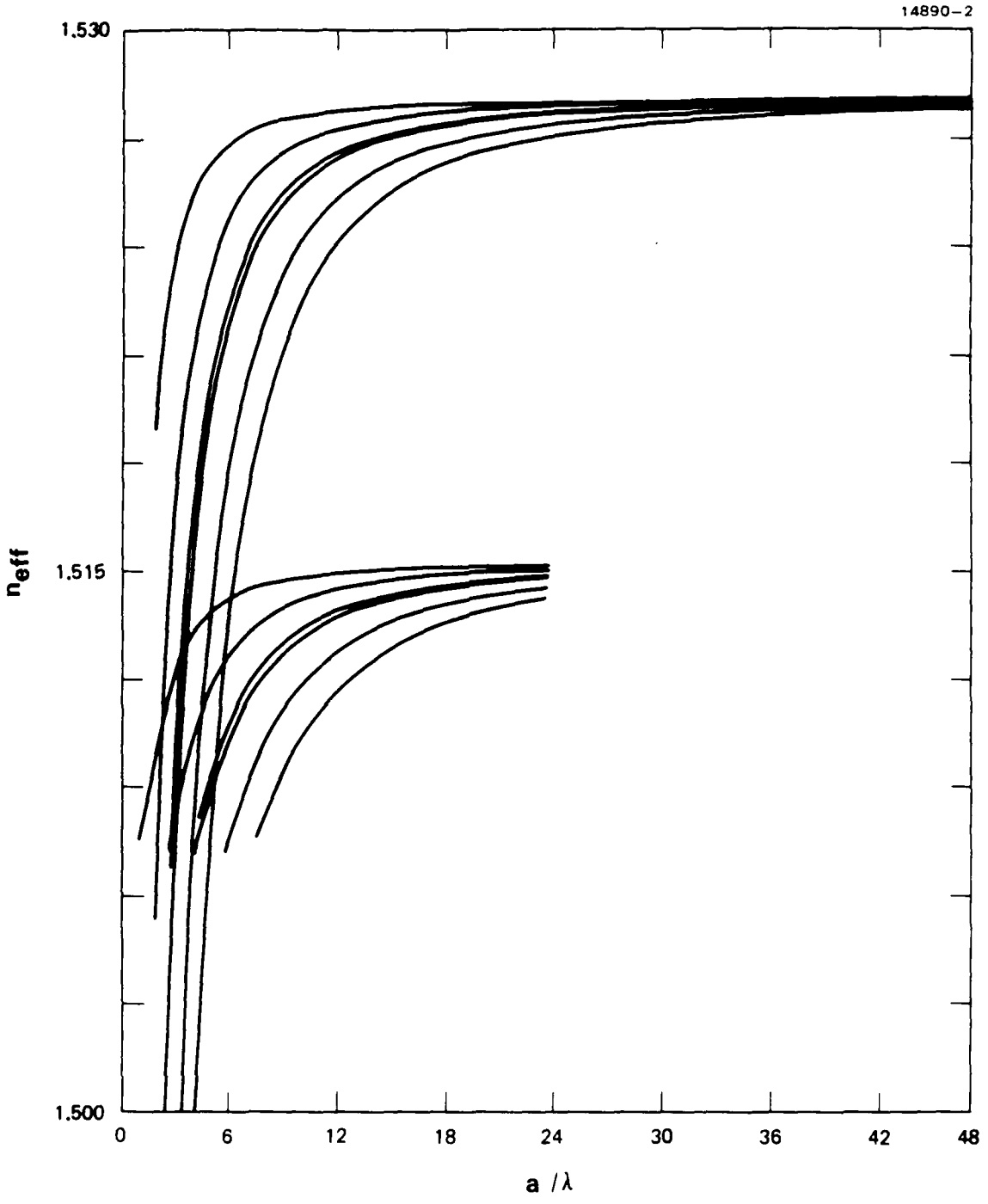

Figure 7. Dispersion curves for hybrid fiber with PK3 glass fiber embedded in an ADP crystal.

core radii specified are in the range of 3 to 5 μm, corresponding to fiber diameters of 6 to 10 μm. As unclad fibers, such core structures would be very difficult to handle without breakage. Thus further modelling is called for to identify wavelength regions in which larger diameter prototype fibers could be used easily for a demonstration of phase-matched SHG. As an alternative we also plan to investigate more rugged "proximal fibers" (see Figure 16) in which a fiber encapsulated in a quartz or copper block is arranged to have a section of its core in direct contact with a nonlinear crystal.

Considerable flexibility has been found to exist in fine-tuning the phase-matching conditions even after construction of a hybrid fiber. This is due to the temperature dependence of the refractive index in all materials. Figure 8 presents the tuning of the phase-matching a/λ value as a function of temperature for the 7052/ADP hybrid considered earlier (Figure 5). For temperature changes of 100 C, 25% variations are possible. Temperature may therefore be a key factor in the laboratory demonstration of SHG.

C. SINGLE-CRYSTAL FIBER GROWTH

1. Traveling Zone Method

The basis of this method is shown in Figure 9. Two sets of synchronously driven wheels move extruded PC fiber through a small heater coil which is used to form a melt with a length between 0.1 and 4 fiber diameters. We find that a horizontal feed of polycrystalline (PC) fiber into the melt zone gives the best control over the diameter of the single-crystal (SC) fiber. In a horizontal position, groove guides provide more mechanical control over the placement of the fiber in the melt zone without applying pressure to the fiber. Since surface tension of the melted fiber is large, we find no sagging of the melt zone even

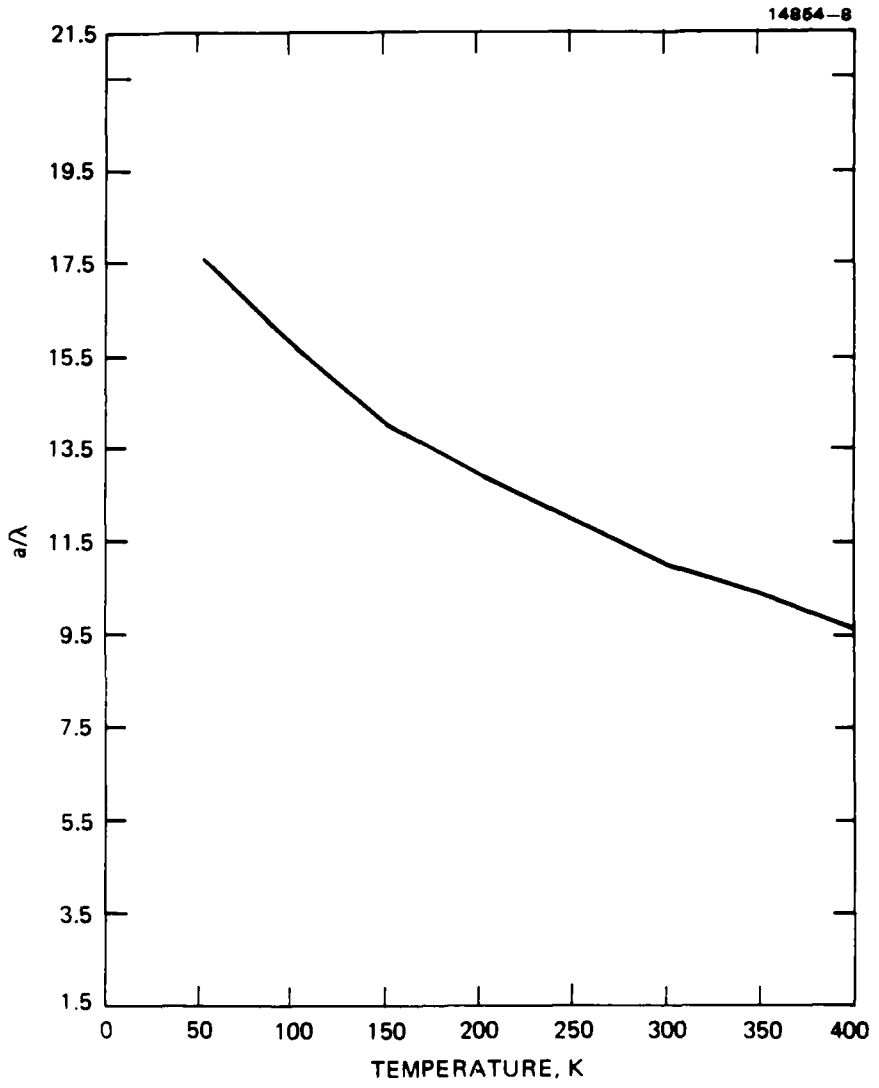

Figure 8. Variation of a/λ phase-matching value with temperature for 7052 glass fiber embedded in an ADP crystal.

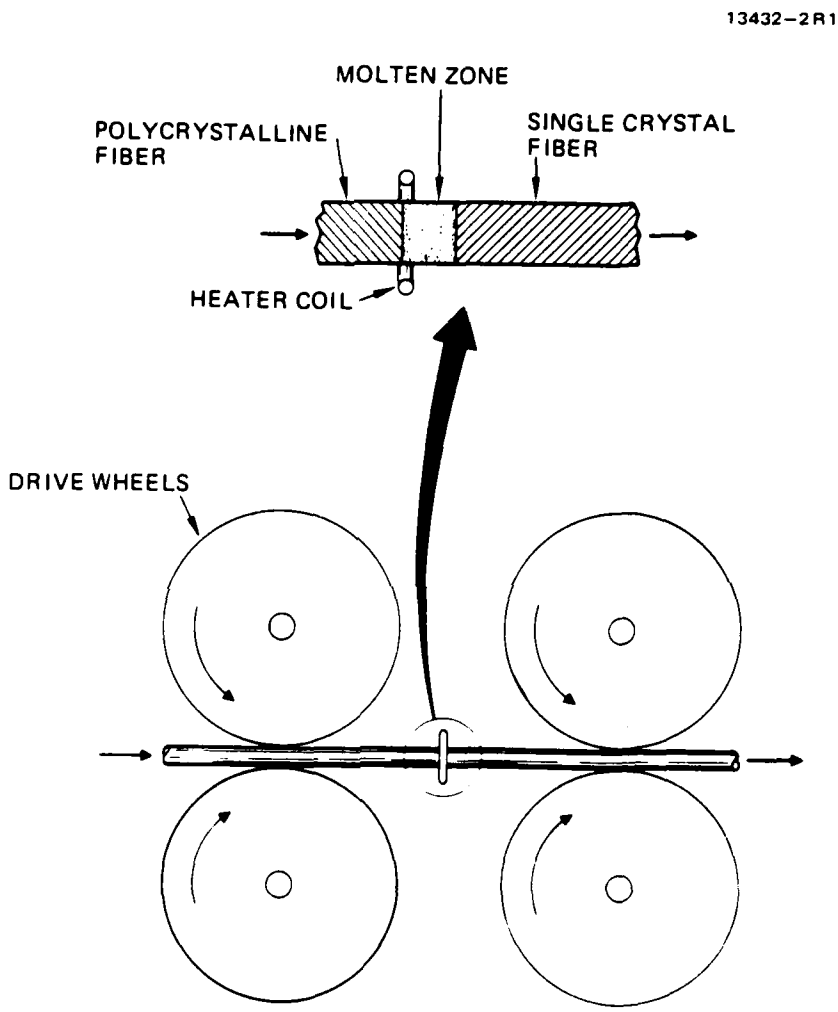

Figure 9. Horizontal traveling-zone fiber growth apparatus.

for horizontally-fed fibers. Our growth rate is approximately 1 cm/min. The fibers grown to date have all nearly preserved the original PC fiber diameter (1:1). Only slight reductions in the SC fiber diameter have been attempted to improve diameter control. However, significant reductions in the final diameters may be possible with simple gear reduction of input and output control wheels.

We have produced SC fibers of AgCl, AgBr, and CuCl by the traveling-zone method. Of these, only CuCl is a nonlinear optical crystal. This growth technique was developed using the less troublesome silver salts which have very low vapor pressure and good resistance to atmospheric contamination at the melting point. In a dry, non-oxidizing atmosphere CuCl is chemically stable at its melting point, but will readily undergo oxidation in moist air to cupric (Cu^{2+}) compounds such as CuO and CuCl(OH). We grew ultrapure water-white crystals of CuCl by the standard Bridgman growth method and used these crystals to produce PC fiber by extrusion. The water-white appearance of the CuCl crystal boules and their lack of near IR absorption demonstrated the lack of Cu^{2+} contamination which would give a telltale bluish color and IR absorption centered at 800 nm. Differential scanning calorimetry of our CuCl crystal showed that it melted at 422 C and transformed to wurzite from a zincblende structure at 407 C (Figure 10). The sharpness of these phase transformation peaks and the lack of other peaks which would not be associated with CuCl is further indication of the purity of our CuCl. PC fibers of CuCl of 1 m in length and 500 μm in diameter were extruded using a standard screw-press technique with a SiC die. Short 10-cm SC fibers of CuCl were made from these PC fibers using a dry nitrogen atmosphere. Longer fibers could not be made with the current setup because the CuCl in the melt zone would occasionally react with atmospheric oxygen, producing a brownish layer on the SC fiber. The traveling zone apparatus should be placed in an oxygen-free dry box in order to achieve long single crystal fibers.

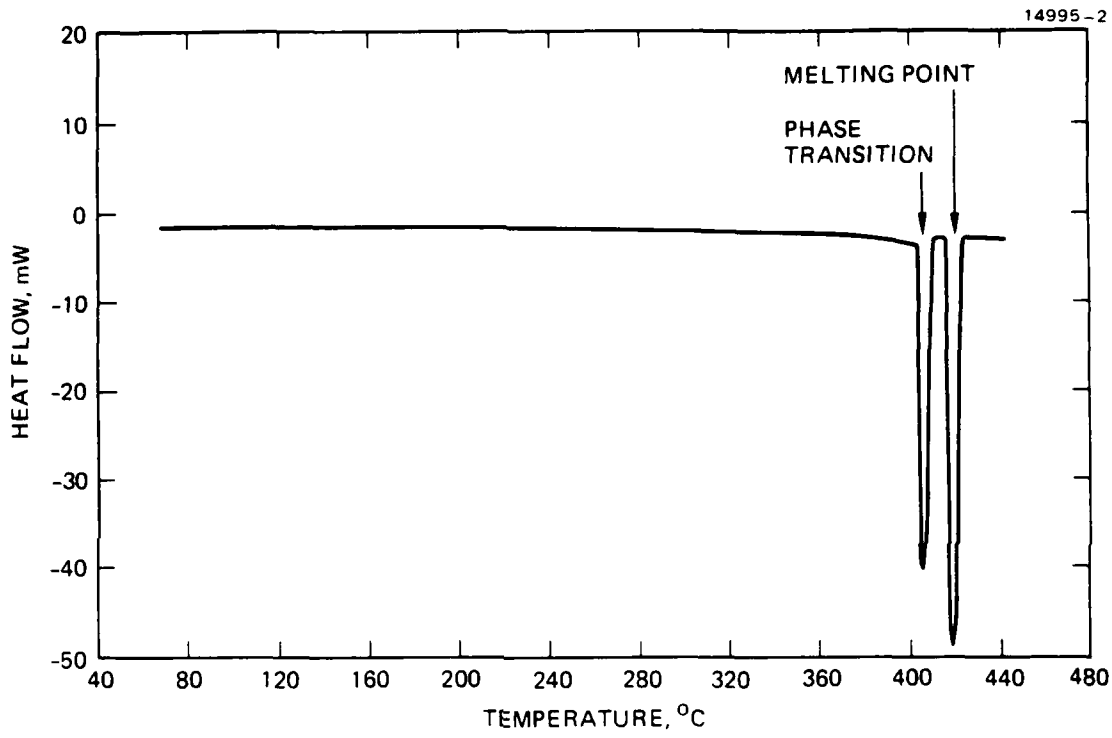

Figure 10. Differential scanning calorimeter thermogram of CuCl single crystal grown at HRL.

A paper on "Single-crystal infrared fibers fabricated by traveling zone melting" was presented at the SPIE Symposium on IR Optical Materials and Fibers, Washington DC, 3-4 May 1984, and published in Proc. SPIE 484, 124 (1984). Appendix A is a reprint of this paper.

2. Capillary-fed Czochralski Method

This method pulls a SC fiber from a melt by using a crucible and die assembly, as illustrated in Figure 11. We developed this growth technique by using nonlinear optical materials having melting points lower than 1000 C, such as $NaNO_2$ and CuCl. This allowed us to fabricate the crucible and die assembly from fused silica, making it possible to view the growth of SC fibers easily within the capillary die, and subsequently to make design modifications following our observations. A description of the capillary-fed Czochralski method was presented at the Sixth American Conference on Crystal Growth, Atlantic City, NJ, on 15-20 July 1984, and is reprinted in Appendix B.

This fiber pulling apparatus had originally been designed for operation in open air, which is compatible with many nonlinear materials including $NaNO_2$, known to be stable in air at its melting point. However, for application to CuCl fiber growth, it had to be redesigned for operation in an inert atmosphere. This new apparatus is shown schematically in Figure 12. The mechanical shutter in the original design has been replaced by an auxiliary heater which plays the role of a thermal shutter. We made numerous attempts to draw SC fibers of CuCl, but the melt invariably turned blue, indicative of Cu^{2+} poisoning. More control on oxygen content in the growth atmosphere is needed to achieve CuCl fiber growth by this method.

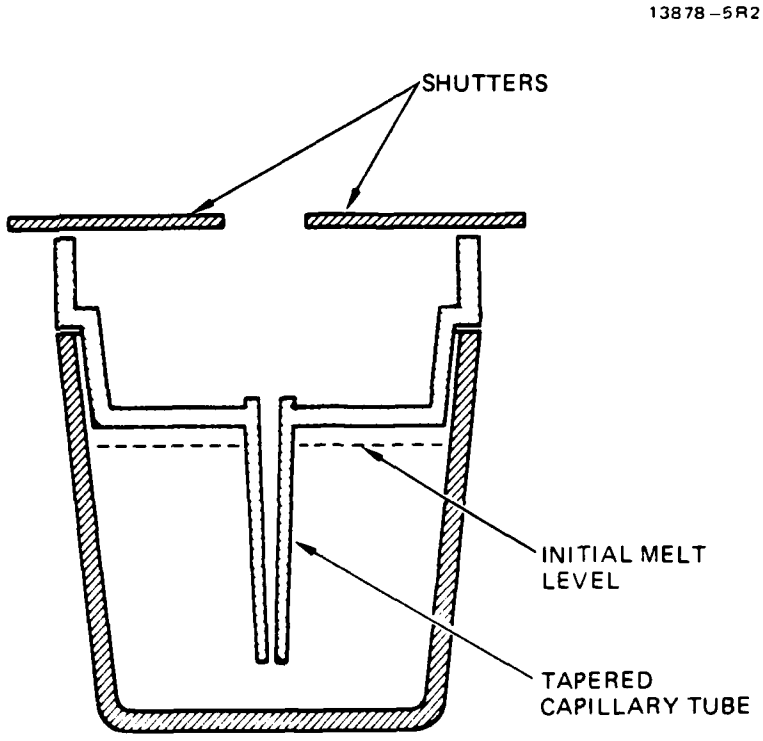

Figure 11. Capillary-fed Czochralski apparatus for growth of single-crystal fibers.

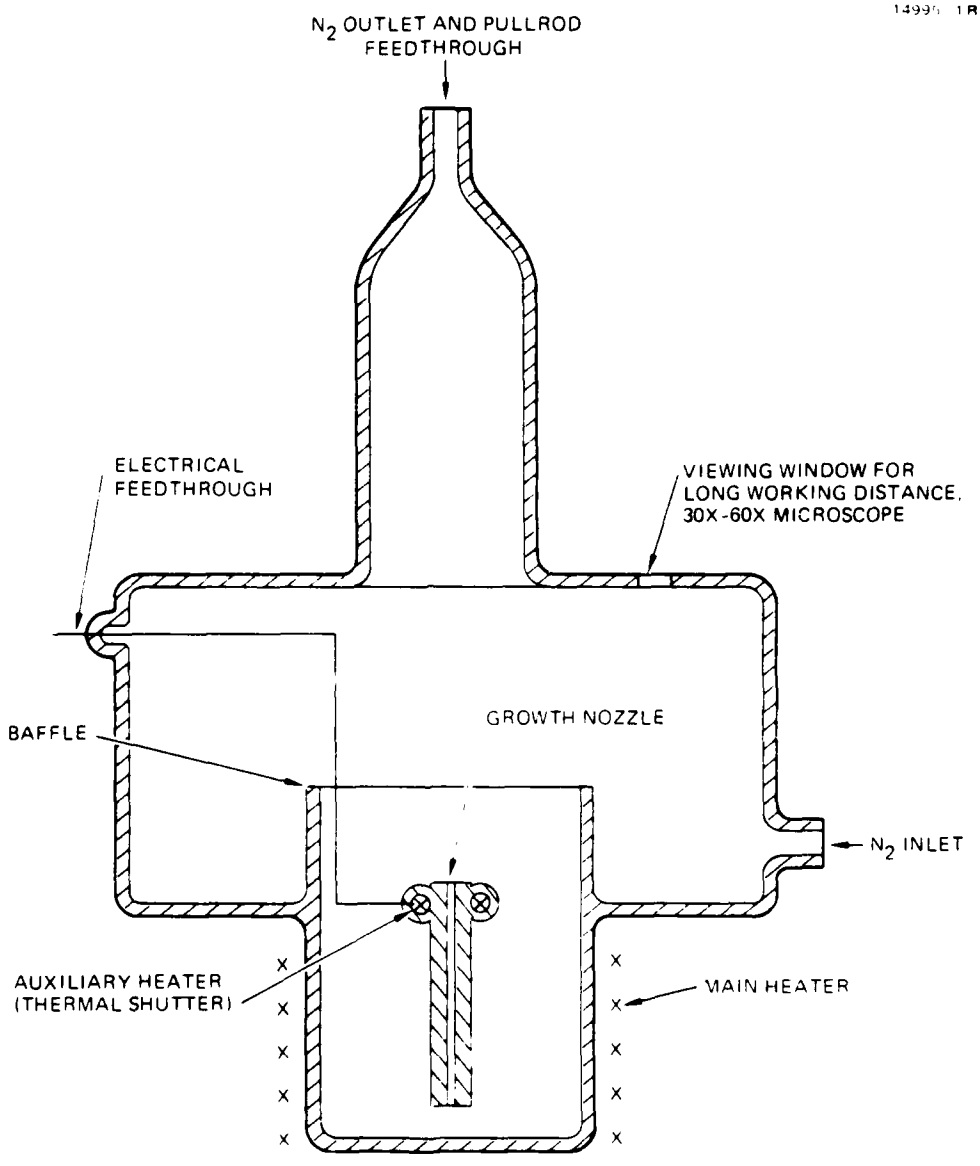

Figure 12. Capillary-fed Czochralski growth apparatus in controlled atmosphere.

SECTION 3

BIOGRAPHIES OF KEY PERSONNEL

The biographies of the personnel who are contributing to the program are presented in the following pages. L.G. DeShazer is the Principal Investigator of this research program.

LARRY G. DeSHAZER, Senior Staff Physicist, Optical Physics Department, Hughes Research Laboratories.

Education — B.S. (Physics), University of Maryland, 1956; Ph.D. (Physics), The John Hopkins University, 1963.

Experience — Dr. DeShazer has 23 years of professional experience in the areas of solid-state lasers, nonlinear optics, laser damage physics, and atomic spectroscopy. From 1963 to 1966 he was at Hughes Aircraft Company, Culver City, involved in research on energy transfer in solid-state laser materials and studies of laser mode selection techniques.

In 1966 he joined the Physics and Engineering Faculty at the University of Southern California as Associate Professor. He was mainly involved in spectroscopy of rare-earth ions in laser materials and pioneered in the measurement of self-focusing parameters by the optical pulse shaping technique and laser damage to thin dielectric films.

In 1973 Dr. DeShazer was appointed the first Director of the Center for Laser Studies at USC, an applied research organization serving as an interface between industry and the university. While on leave of absence from USC, from 1975 to 1976, he was Liaison Scientist with the U.S. Office of Naval Research, London. He left USC in 1978 to return to Hughes at the Research Laboratories with responsibilities in solid-state laser and nonlinear optics research programs.

Honors — Fellow of Optical Society of America; Gilman Fellow at John Hopkins University (4 years); Phi Kappa Phi; Phi Eta Sigma; Sigma Pi Sigma; Gamma Alpha.

Professional — American Physical Society, Optical Society of America; The Royal Institution of Great Britain,; Sigma Xi, IEEE Group of Electron Devices; SPIE.

Publications — Dr. DeShazer is the author of 108 technical papers in the fields of solid-state lasers, nonlinear optics and spectroscopy. He has 3 patents in solid-state lasers, and was the dissertation chairman for twenty Ph.Ds.

ANTONIO C. PASTOR, Member of the Technical Staff, Optical Physics Department, Hughes Research Laboratories.

Education — B.S. (Chemical Engineering), University of Santo Tomas (Manila, Phillipines), 1950; M.S. (Physics), University of Chicago, 1958.

Experience — Mr. Pastor joined Hughes in 1968 and has been involved in the growth of refractory laser and electro-optic crystals, as well as the design of growth equipment for use in the Hughes Reactive Atmosphere process for highly transparent alkali halide and alkaline earth fluoride window material. More recently he has been involved in similar work on monocrystalline fiber growth of potassium and thallium halides and in the deposition of thin films of inorganic compounds using metallo-organic photoresists. From 1961 to 1968 he was employed at Korad, working on improving the Verneuil method of crystal growth and also on the development of high temperature crystal preparation methods and the related ceramics and instrumentation techniques. Earlier, he was an instructor at the University of Santo Tomas and at the Montana School of Mines; he also practiced chemical engineering and operated a commercial laboratory for chemical analysis. More recently, he has been teaching courses in materials science at Santa Monica College and West Coast University.

Professional Societies — American Association of Crystal Growers; American Association for the Advancement of Science.

Publications — Mr. Pastor is the author of several papers in the Journal of Chemical Physics, the Materials Research Bulletin and other publications. He has numerous patents and patent disclosures in the field of crystal growth.

STEPHEN C. RAND, Member of the Technical Staff, Optical Physics Department, Hughes Research Laboratories.

Education

B.Sc. (Physics), McMaster University, 1972;
M.Sc. (Physics), University of Toronto, 1974;
Ph.D. (Physics), University of Toronto, 1978.

Experience

Prior to joining Hughes, Dr. Rand was engaged in light scattering experiments at the University of Toronto, reporting Brillouin measurements in all the rare gas solids and the family of deuterated methane compounds. He spent two years as a World Trade Fellow at IBM Research in San Jose, California where his research was in the area of optical coherent transients and spectral hole-burning in rare-earth doped crystals. This was culminated in the discovery of "magic-angle line narrowing" on an optical transition of Pr ions in LaF_3. He subsequently spent two years as a research associate in the Stanford University Department of Physics where he studied up-conversion radiation by trios of interacting ions in rare earth materials.

Since joining Hughes Research Laboratories in June 1982, Dr. Rand has demonstrated three new tunable solid state lasers, including the diamond laser which is the first color center laser to operate stably at room temperature. He has also performed continuous wave phase conjugation and four-wave mixing experiments in a variety of rare earth and transition metal compounds, and in color center materials for the first time. He is currently involved in experimental work in the areas of fiber optics, nonlinear optics, color center lasers, stimulated pair processes, and optical coherent transients.

Professional Societies

American Physical Society; Optical Society of America.

Publications

Dr. Rand's publications in the above areas include more than 20 papers. He has also contributed to several books: Laser Spectroscopy IV (1979), Laser Spectroscopy V (1981), Light Scattering in Solids (1979), and Lasers and Applications (1981).

REFERENCES

1. S.C. Rand, "Nonlinear optical devices using embedded optical fibers," Patent Disclosure No. PD83307, Sept. 8, 1983.

2. G. Hewig and K. Jain, J. Appl. Phys. 54, 57 (1983).

3. A.Y. Cabezas, L.G. Komai, and R.P. Treat, Appl. Opt. 5, 647 (1966).

4. K.E. Wilson, Ph.D. dissertation (Physics), University of Southern California, Jan. 1980.

5. K.E. Wilson and L.G. DeShazer, in Basic Optical Properties of Materials (NBS Special Publication 574, May 1980), p. 85-86.

6. D. Gloge, Appl. Opt. 10, 2252 (1971).

APPENDICIES

APPENDIX A

Published in Proc. SPIE 484, 124 (1984)

J.A. Harrington,* A.G. Standlee, A.C. Pastor, and L.G. DeShazer

Hughes Research Laboratories, 3011 Malibu Canyon Road
Malibu, California 90265

Abstract

Single crystal fibers of thallium, silver and cuprous halides have been fabricated by passing polycrystalline extruded fibers through a small submillimeter melt zone, converting them to single crystal fibers. The lowest loss measured in a single-crystal fiber was 6.6 dB/m at 10.6 μm for AgBr, 620 μm in diameter and 80 cm in length.

Introduction

Extruded, polycrystalline (PC) infrared fibers have been successfully employed in a variety of short-length (<10 m) sensor and power delivery applications.[1] The losses in the metal halide PC fibers, however, are well above their theoretical intrinsic loss of 10^{-3} dB/km near 5 μm. For example, the best PC fiber[2] is thallium bromoiodide (KRS-5) which has a loss of 190 dB/km at 10.6 μm, several orders of magnitude above the intrinsic limit at this wavelength. The large extrinsic attenuation in PC waveguides results from grain boundary effects such as absorption and scattering from impurities decorating boundaries, residual strain induced in the fibers during extrusion, and poor fiber surface quality.

Single-crystal (SC) fibers have the potential of eliminating all the deleterious effects of extruded fiber and, therefore, of having much lower loss than PC fibers. In addition, SC fibers would lead to new nonlinear fiber optic applications. By minimizing fiber strain and by growing fiber with smooth surfaces we expect greatly reduced scattering losses. In this paper we report a new method of SC fiber fabrication in which PC fiber is converted into SC using a traveling-zone growth technique. Using this method, we have made 1-m long lengths of silver and thallium halide SC fibers with losses as low as 6.6 dB/m at 10.6 μm.

Background

Previous SC fiber growth techniques have, in general, relied on a capillary shaper or edge-definer to configure the fiber diameter. Bridges et al.[3] pulled AgBr fibers upward through a capillary while Ota et el. pulled KRS-5[4] and CsI[5] fibers downward through a shaper. Earlier work at Tyco Labs[6] and by Stepanov[7] used edge-defined capillary growth for SC sapphire fiber. In all these cases, a molten reservoir of material was used as a source. In our traveling zone method, using unencapsulated PC fiber, we do not use a shaper and, therefore, no part of the molten zone contacts a surface. We thus eliminate a potential impurity source which occurs when the melt contacts the container walls. Another advantage of our method is that the melt zone is very small, approximately one fiber diameter in length. This advantage is also a feature of the work of Feigelson et al.[8] who use laser heating to melt a small portion of a crystal rod in a pedestal growth scheme. In this case, however, there are problems in controlling the fiber diameter because there is no shaper and there is a 3:1 diameter reduction from feed stock to fiber.

Traveling Zone - Encapsulated SC Fiber Growth

Our approach to SC fiber growth is quite different from the usual melt-shaper and pedestal methods. Instead of beginning with a melt, we begin with extruded PC fiber which we convert to SC fiber using a traveling-zone technique. The advantage of starting with an extruded fiber to produce a SC fiber is that the method is scalable to long fiber lengths, and diameter control may be easier than in the melt-related methods. To study the feasibility of converting a PC to a SC fiber, we carried out a series of experiments on PC fibers encapsulated in quartz capillary tubes. To convert the PC fibers to SC fibers, the fibers were heated to just below, or slightly above, the melting point (MP). While this particular approach is not readily scalable to long SC fiber lengths, the information gained in these experiments was useful in developing the related SC fiber.

Figure 1 shows the salient features of the growth setup. The 500-μm-diameter KRS-5 fiber is placed in a close-fitting capillary (precision bore, fused quartz) and sealed at both ends. For some experiments the capillary is evacuated, and for others a small amount of He gas is added. The tube was passed through heaters arranged in both a horizontal and vertical geometry. Since little difference was observed, most experiments were made by passing the tube vertically downward through the heater coils. The tube and fiber were passed through the heater coil from one to three times at speeds ranging from 1 to 3 mm/hr.

*Now at Infrared Fiber Industries, 2500 Townsgate Rd., Unit J, Westlake Village, CA 91361.

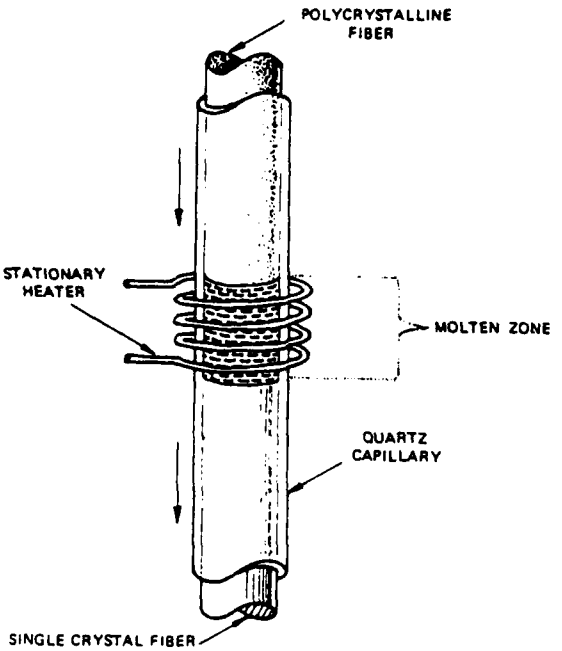

Figure 1. Traveling zone method of SC fiber growth in which PC fibers are encapsulated in a quartz capillary.

The resulting fibers were SC when the fiber was heated to above the MP (410°C for KRS-5). Heating below the MP left the fiber with SC regions about 1 mm long. That is, we could not propagate the grain boundaries for the full length of the fiber. For those fibers that were melted, we found that the surface quality was very poor. Bubbles formed on the surface as a result of trapped gas and the surface was generally dull due to the wetting that occurred between the quartz and KRS-5. In fact, surface tension was so great that the fibers did not contract sufficiently on cooling to permit easy removal of the fiber from the tube. We, therefore, terminated this approach in favor of an unencapsulated-fiber traveling-zone method.

Traveling Zone – Unencapsulated SC Fiber Growth

The heart of this method is sketched in Figure 2. Two sets of synchronously driven drive wheels move extruded PC fiber through a small heater coil which is used to form a melt zone with a length between 0.1 and 4 fiber diameters. As surface tension of the melted fiber is large, we find no sagging even if growth is horizontal. Our growth rate is approximately 1 cm/min. The fibers grown to date have all preserved the original PC fiber diameter (1:1) but we see no difficulty in making slight reductions in the SC fiber diameter by independently driving the two sets of wheels.

As an interesting aside, we note that it is also possible to surface or skin melt the PC fiber. We have done this for 620-μm diameter AgBr fiber to a skin depth of about 20% of the fiber diameter. The resultant fiber has a single crystal outer layer and a large grain polycrystalline core. The advantage of only a skin melt would be the added strength afforded by a PC core and for the improvement of the surface quality of PC fibers.

The extruded PC fibers we have converted into SC fibers include Tl_2BrI (KRS-5), TlBr, CuCl, AgCl, and AgBr. The thallium salts pose a problem because the vapor pressure of these salts is high and the resultant SC fiber surface is dull due to thermal etching. For the first time, PC fibers of CuCl of 1-m length and 500 μm diameter were extruded from a water-white single crystal grown at HRL from which SC fibers of CuCl were produced. However, because the conversion of PC to SC fiber was conducted in air, the melt surface reacted with the atmospheric oxygen producing a mottled brownish layer on the SC fiber. A chamber surrounding the melt zone is currently being constructed to control both the high vapor pressure and reaction problems of these materials.

Initially our best results were obtained for the silver salts which have a very low vapor pressure and good resistance to atmospheric contamination at the melting point. As an example of our results, we chose

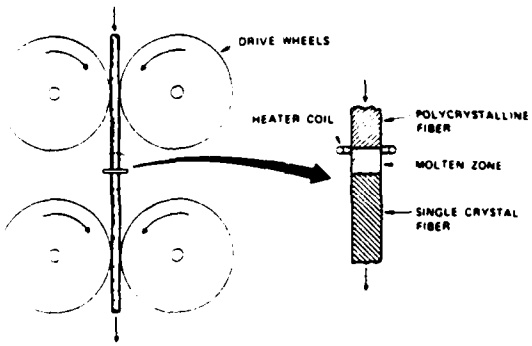

Figure 2. Traveling zone growth of SC fibers without encapsulation (vertical fiber position).

AgBr. Extruded AgBr, 620-μm diameter, traveled through a melt zone one fiber diameter in length obtained with a single-turn heater power of 0.87 W. The solidus-liquidus interface remained quite stationary during growth and meter long lengths are possible without any adjustment of the initial growth parameters. The results of our optical absorption measurements at 10.6 μm are given in Table 1.

Table 1. AgBr Fiber Loss at 10.6 μm

PC Fiber		SC Fiber	
Length (cm)	Loss (dB/m)	Length (cm)	Loss (dB/m)
94	2.6	80	6.6
49	8.5	28	8.3

We note for the longer fiber that the total attenuation is less for the starting PC fiber than for the converted SC fiber. This, plus the face that the lowest loss of 6.6 dB/m is still rather high, is due to some irregularities in the fiber surface quality and a few bubbles included in the fiber core. We expect these losses to be reduced by better control of the fiber drive, by stabilization of the temperature, and by using an inert ambient environment around the melt zone.

The orientation of the single crystal fiber was most simply obtained by using the preferential-etch method of Bridges et al.[3] In Figure 3 we show a section of fiber surface etched in 30% sodium thiosulphate for two minutes. The (110) direction is matte and the (100) direction is shiny. This indicates that the growth axis is along the (100) direction. By sampling pieces along the length of the fiber, we determined that the entire fiber grows in this orientation. These results are also confirmed by slightly stressing the fiber. Figure 4 shows the (110) slip planes which result from tensile stress applied along the fiber axis.

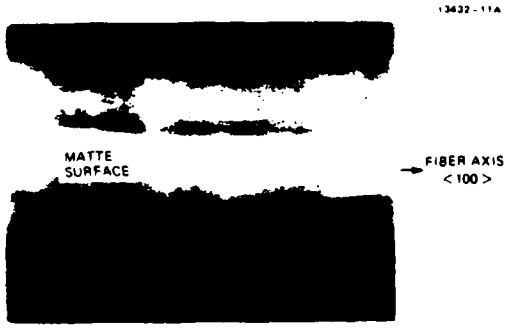

Figure 3. SC fiber of AgBr etched in 30% sodium thiosulphate solution to reveal (110) matte and (100) shiny directions. 100X magnification.

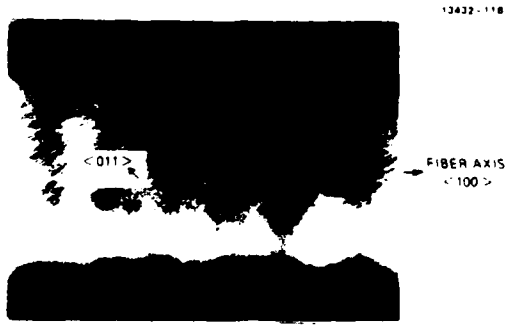

Figure 4. SC fiber of AgBr stressed to reveal (110) slip planes. 100X magnification.

Conclusion

A unique feature of our SC fiber growth method is that we begin with fiber to make fiber. We feel that this has advantages over other SC fiber fabrication methods which generally involve a large melt reservoir. Furthermore, our containerless, non-contact method is clearly scalable to long fiber lengths. Finally, the method lends itself to the production of SC fibers from congruently melting, nonlinear and electro-optic materials. Such nonlinear or EO fibers would be useful in laser frequency and modulator applications.

Acknowledgments

The authors acknowledge the assistance of R.R. Turk in the initial stage of development of this traveling zone method. This work was supported by AFOSR contract No. F49620-82-C-0030.

References

1. Harrington, J.A., "Crystalline Infrared Fibers," Infrared Fibers, Proc. of Soc. Photo-Opt. Instr. Eng., Vol. 266, pp. 10-15, 1981

2. Harrington, J.A. and Standlee, A.G., "Attenuation at 10.6 μm in Loaded and Unloaded Polycrystalline KRS-5 Fibers," Appl. Opt., Vol. 22, pp. 3073-3078, 1983.

3. Bridges, T.J. et al., "Single-Crystal AgBr Infrared Optical Fibers," Opt. Lett., Vol. 5, pp. 85-86, 1979.

4. Mimura, Y. et al., "Growth of Fiber Crystals for Infrared Optical Waveguides," Jap. J. Appl. Phys., Vol. 19, pp. L269-L272, 1980.

5. Okamura, Y. et al., "CsI Crystalline Fiber for Infrared Transmission," Jap. J. Appl. Phys., Vol. 19, pp. L649-L651, 1980.

6. LaBelle, H.E., Jr., et al., "EFG, The Invention and the Application to Sapphire Growth," J. Crys. Growth, Vol. 50, pp. 8-17, 1980.

7. Antonov, P.I. et al., "Physical Problems in Crystal Growth by the Stepanov Method," J. Crys. Growth, Vol. 50, pp. 3-7, 1980.

8. Fejer, M. et al., "Growth and Characterization of Single-Crystal Refractory Oxide Fibers," Advances in Infrared Fibers II, Proc. SPIE, Vol. 320, pp. 50-55, 1982.

APPENDIX B
Presented at VI American Conference on Crystal Growth, Atlantic City, NJ, July 1984. To be published in J. Crys. Growth

Journal of Crystal Growth 70 (1984) 295–299
North-Holland, Amsterdam

SINGLE CRYSTAL FIBER DRAWING

A.C. PASTOR

Hughes Research Laboratories, Malibu, California 90265, USA

In this paper a novel method of growing from the melt single crystal fibers (SCF) of congruently melting compounds is described. This SCF growth method is characterized by the absence of an interface between the melt and its vapor from the vicinity of the growth interface during the growth process, so that the surface tension of the melt plays no role in determining the periphery of the growth interface, and the shaper functions as a die. This method is distinct from previously reported SCF growth methods, and, unlike the latter, has no analogue among the established methods of bulk single crystal growth. Because of its similarity to the process of metal wire forming we call this method of SCF growth the drawing method.

1. Introduction

The Bridgman and the Czochralski methods of growing bulk single crystals from the melts of congruently melting compounds involve four material phases, viz. the crystal, the melt, the vapor, and the container or crucible. Bridgman and Czochralski systems have only five of the six possible interfaces among four phases. The Bridgman system is characterized by the absence of a crystal–vapor interface, the Czochralski system by the absence of a crystal–container interface.

In the domain of shaped crystal growth the Stepanov method, as described by Antonov and Nikanorov [1], or the Edge-defined Film-fed Growth (EFG) method, as described by LaBelle [2], involves the same four phases, and is characterized by the absence of the crystal–container interface. Either method may therefore be regarded as a derivative form of the Czochralski method. This observation is not new, and the similarity has been quite explicitly indicated by Cullen and Surek [3]. On the same basis of comparison the methods of SCF growth employed by Bridges et al. [4] with silver halide and by Mimura et al. [5] with cesium and thallous halides are also Czochralski-derived methods.

The method of SCF growth that is the subject of this paper is distinct from the Stepanov or the EFG method in that it has no melt–vapor interface surrounding the growth interface, and therefore cannot be regarded as a derivative form of the Czochralski method. Neither is it a derivative form of the Bridgman method because of the presence in it of a crystal–vapor interface. There is direct physical contact between crystal and shaper during growth, and the shaper truly functions as a die. This method has no analogue among the established methods of bulk single crystal growth.

2. Design of the apparatus

This method of SCF growth makes use of a crucible and die assembly such as that illustrated in cross section in fig. 1a. For growth materials with melting points below 1000°C this assembly could be fabricated from vitreous silica. The die was made by drawing a piece of heavy-walled capillary tubing and cutting from it a piece that had an internal diameter which tapered from 0.8 mm at one end to 0.3 mm at the other. A pair of ordinary microscope slide glasses served adequately as shutters, the function of which was to provide control of the axial thermal gradient in the die.

This SCF growth apparatus was designed for operation in open air and could not be used with melts that were sensitive to moist air. Work is currently in progress to incorporate reactive atmosphere processing (RAP) [6] into the design of the appara-

0022-0248/84/$03.00 Elsevier Science Publishers B.V.
(North-Holland Physics Publishing Division)

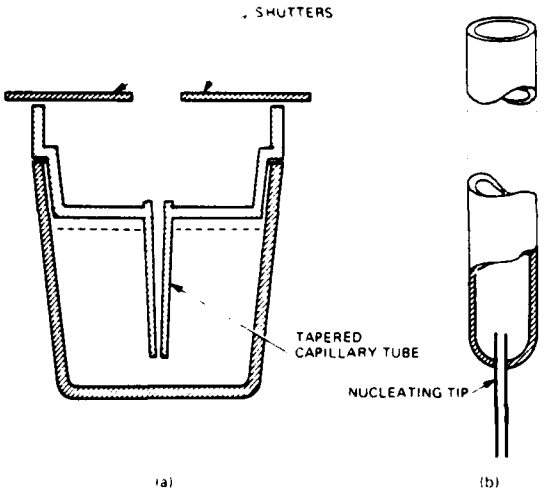

Fig. 1. (a) Crucible and die assembly. (b) Crystal pulling rod

tus. RAP SCF growth will greatly broaden the spectrum of growth materials to which this method will be applicable.

The crystall pulling rod is hollow from end to end. It was originally made of borosilicate glass tubing with a nucleating tip of thin-walled capillary platinum tubing, as is shown in fig. 1b. The platinum tubing had an inside diameter of 0.18 mm and an outside diameter of 0.25 mm. An alternative design of the pulling rod consisted of vitreous silica tubing that was drawn at one end to 0.25 mm diameter. Its nucleating tip was quite fragile, and required great care in alignment with the die orifice at the start of each fiber drawing run. If it broke in the orifice accidentally, the die had to be replaced, and a large part of the start-up procedure had to be repeated.

The furnace used was simply constructed from a stack of firebricks which was hollowed out to accommodate a pair of semicylindrical Kanthal-wound heating elements. Touch-up insulation with Kaowool was applied until a chromel–alumel control thermocouple indicated sufficient thermal stability.

3. Description of procedure

The dashed line in fig. 1a indicates the level of melt to which the crucible was charged before a series of fiber growth runs was started. Due to capillary action the die filled up with melt to the top. The crucible-and-die assembly was so positioned in the upright clamshell heater that the charge material was just completely melted with the shutters in the closed position but crystallized at the die orifice with the shutters in the fully opened position. The depth of crystallization in the die could then be controlled with the width of the opening between the shutters.

Fig. 2 shows the simplified method of operation of the system with a sequence of diagrams. Only the cross section of the system in the region of the growth interface is shown in each of the diagrams in the sequence. Fig. 2a depicts the system at the moment of contact of the tip of the pulling rod with the melt, during which time the shutters are in the closed position. Melt rises some distance into the nucleating tip by capillary action before it encounters a temperature low enough to cause it to crystallize spontaneously and prevent further capillary climb. The shutters are then partly opened so that the top layer of melt in the orifice may crystallize to a crust. This is indicated by a change in the texture and the gloss of the exposed surface of the material. Fig. 2b shows the system at that stage. Crystal pulling may then be started. Fig. 2c shows the system moments after that

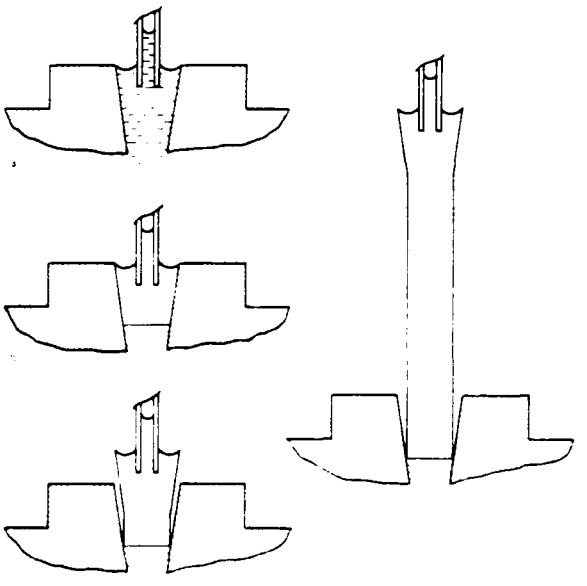

Fig. 2. Method of operation of SCF drawing system, greatly simplified

has been done, and fig. 2d shows it at a much later stage, when steady-state SCF growth is well underway. Note in figs. 2c and 2d that there is no melt–vapor interface during growth of the SCF.

A typical SCF drawing run is not quite as straightforward as fig. 2 would indicate. To achieve steady-state growth a scan had to be made of pulling rates in order to determine the steady-state value of that parameter. If that value was exceeded, melt would periodically seep through past the growth interface and freeze onto the fiber. A fiber grown under such conditions would have an irregular, polycrystalline surface. If the fiber was pulled at less than the steady-state growth rate, the growth front would advance deeper into the die, the solid-to-solid contact surface, i.e., the crystal–die interface, would increase, and the resistance to the pull would eventually exceed the tensible strength of the fiber. Even before the fiber snapped, it could lose its crystalline integrity when the tension exceeded its yield strength. In scanning for the steady-state drawing rate, it was therefore preferable that the approach to that value be made from the fast end of the range of drawing rates. Steady-state growth would be achieved when the fiber grew with constant diameter.

Depending on the taper in the die, the diameter of the fiber may be caused to decrease by opening the shutters wider at that stage of the fiber growth run depicted in fig. 2c. If this were done at that stage of fig. 2b, the resistance to pull may become great enough to sever the crystal from the pulling rod.

A further feature of some significance of this SCF growth system is that the growth end of the fiber is held rigidly in place by the die, thus obviating the need for alignment devices, which are essential to Stepanov or EFG SCF growth systems. Any instability due to transverse vibrations of the growing fiber, which will magnify as the grown fiber lengthens, will pose no problem in spite of the absence of such alignment paraphernalia.

Two methods were considered for smoothening the surface of the grown fiber: heat polishing and chemical milling. The latter alternative was chosen for two reasons: (1) it was far simpler to reduce to practice, and (2) it offered an added dimension in the form of controllable reduction of fiber diameter. The selection of milling reagent will depend on the fiber material and will be covered in the next section.

4. Materials selection

Plastic deformation of a SCF will alter its defect structure and, presumably, its optical properties. Materials with low melting points have relatively poor mechanical properties. In particular, low-melting materials with cubic structure have low yield strengths. For example, single crystals of potassium chloride have a yield strength-to-Young modulus ratio of around 10^{-4}, and therefore a 100 μm fiber of this material cannot be bent to a radius of curvature less than 1 meter without deforming it permanently. For lower melting materials such as silver, cesium, and thallous halides, the minimum limit of the radius of bend curvature would be even greater. Such considerations had to be taken into account in the process of selection of a growth material.

Sodium nitrite ($NaNO_2$) was selected as the test material with which to establish the viability of this method of SCF growth. This compound melts congruently at 271 °C, and its melt is stable in air up to around 320 °C, above which temperature it will decompose [7]. When the grown crystal of sodium nitrite is cooled down past 160 °C, it will undergo a first-order transition to a ferroelectric phase [8]. Because of its possible use in nonlinear optics experiments, sodium nitrite SCF would not have to be grown to transmission-line lengths of many meters.

A sodium nitrite crystal of moderate bulk will decrepitate as it undergoes the solid-to-solid transition at 160 °C. However, since the free surface of a crystal will remain stress-free through such a transition, it was deemed reasonable to expect that decrepitation might not occur in a SCF as a consequence of its high surface-to-volume ratio. This speculation seems to have been proved correct by the experimental results.

For fast milling action on the grown fiber of sodium nitrite the milling reagent selected was isopropyl alcohol. If slower solvent action were desired for closer control of fiber diameter, a second choice of milling reagent was ethylene glycol. A still slower solvent would be glycerine.

5. Experimental results

SCF of sodium nitrite were successfully grown by the method just described. Fig. 3 shows a fiber drawing run in progress. The diameters of the fibers

Fig. 3. Single crystal fiber drawing in progress.

grown ranged from 0.2 to 0.5 mm. Two dies with bores of different size were used. At the smaller diameters the fiber would snap before it could be grown to a length of 10 cm, but the reason for this may have been that even the fastest drawing rates applied were not fast enough.

At the larger diameters the lengths of the fibers grown were limited only by the range of the crystal pulling mechanism that was used. The longest fiber with a diameter of 0.5 mm, grown in two stages with minor interruption in between, was more than 60 cm long. It was grown at a linear growth rate of 1.5 cm/h, which was typical for that diameter. Fig. 4 shows a segment of 0.5 mm fiber as grown. For longer SCF lengths the pulling mechanism could have been replaced with a reel having a radius greater than the nondeforming minimum radius of bend curvature of the fiber.

Preliminary experimentation on chemical milling was performed with absolute isopropyl alcohol as the milling reagent. Fibers were milled down to 120 μm by the crude method of repeated dunking. Fig. 5 shows a segment of such a fiber. The handling of sodium nitrite fiber with such a diameter is difficult, and the incidence of breakage is high. The in-

Fig. 4. Segment of sodium nitrite fiber as grown. Diameter = 500 μm.

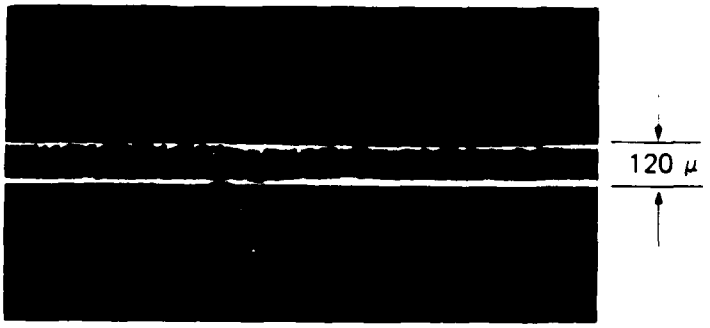

Fig. 5. Segment of sodium nitrite fiber after chemical milling. Diameter = 120 μm.

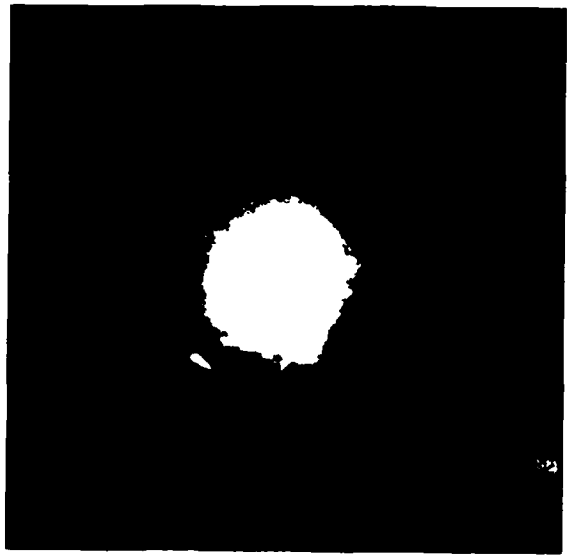

Fig. 6. Laue photograph of milled sodium nitrite fiber.

dications are that the desired milling rates are between those that isopropyl alcohol and ethylene glycol can provide. A mixture of these two solvents should be used as the milling reagent for closer diameter control. However, the handling problems will have to be overcome before the refinements of the milling operation can gain importance.

Fig. 6 is a Laue photograph showing monocrystallinity of the sodium nitrite fiber after milling. For lack of a practical method to establish the crystalline integrity of these fibers, this index to their quality has not been determined.

6. Conclusion

We have demonstrated the feasibility, as well as the convertibility to production scale, of a new SCF growth and finishing method with practically no limitation on fiber length.

Acknowledgements

The author is grateful to Ch. Fetters and L. Veit for the excellent glassblowing craftsmanship they provided, to F.V. Lee for his assistance in other aspects of this project, and to S.C. Rand for the loan of the photographs in figs. 4, 5 and 6. This work has been funded in part by AFOSR.

References

[1] P.I. Antonov and S.P. Nikanorov, J. Crystal Growth 50 (1980) 3.
[2] H.E. LaBelle, Jr., J. Crystal Growth 50 (1980) 8.
[3] G.W. Cullen and T. Surek, J. Crystal Growth 50 (1980) vii.
[4] T.J. Bridges, J.S. Hasiak and A.R. Strnad, Opt. Letters 5 (1979) 85.
[5] Y. Mimura, Y. Okamura, Y. Komazawa and C. Ota, Japan. J. Appl. Phys. 19 (1980) L269.
[6] R.C. Pastor and A.C. Pastor, Mater. Res. Bull. 10 (1975) 117.
[7] Handbook of Chemistry and Physics, 61st ed. (Chemical Rubber Publ. Co., 1980).
[8] F. Jona and G. Shirane, Ferroelectric Crystals (Pergamon, 1962).

END

FILMED

3 -86

DTIC